

The role of coseismic Coulomb stress changes in shaping the hard-link between normal fault segments.

M. Hodge¹, Å. Fagereng¹, J. Biggs²

Michael Hodge, hodgems@cardiff.ac.uk

¹School of Earth and Ocean Sciences,
Cardiff University, Cardiff

²School of Earth Sciences, University of
Bristol, Bristol

This article has been accepted for publication and undergone full peer review but has not been through the copyediting, typesetting, pagination and proofreading process, which may lead to differences between this version and the Version of Record. Please cite this article as doi: 10.1002/2017JB014927

Abstract. The mechanism and evolution of fault linkage is important in the growth and development of large faults. Here we investigate the role of coseismic stress changes in shaping the hard-links between parallel normal fault segments (or faults), by comparing numerical models of the Coulomb stress change from simulated earthquakes on two en echelon fault segments to natural observations of hard-linked fault geometry. We consider three simplified linking fault geometries: 1) fault bend; 2) breached relay ramp; and 3) strike-slip transform fault. We consider scenarios where either one or both segments rupture and vary the distance between segment tips. Fault bends and breached relay ramps are favoured where segments underlap, or when the strike-perpendicular distance between overlapping segments is less than 20% of their total length, matching all 14 documented examples. Transform fault linkage geometries are preferred when overlapping segments are laterally offset at larger distances. Few transform faults exist in continental extensional settings, and our model suggests that propagating faults or fault segments may first link through fault bends or breached ramps before reaching sufficient overlap for a transform fault to develop. Our results suggest that Coulomb stresses arising from multi-segment ruptures or repeated earthquakes are consistent with natural observations of the geometry of hard-links between parallel normal fault segments.

Keypoints:

- We investigate Coulomb stress change between two parallel, unconnected fault segments =

- CSC from multi-segment ruptures or repeated earthquakes are consistent with natural observations of normal fault hard-link geometry. =
- Fault link type depends on the relative geometry of the segments at the inter-segment zone =

1. Introduction

Large continental faults - those whose lengths are much greater than the seismogenic thickness they reside within - typically comprise a number of smaller fault segments [e.g. *Schwartz and Coppersmith*, 1984; *Wesnowsky*, 1986; *Peacock and Sanderson*, 1991], defined here as a portion of a master fault or fault zone. The number of ‘major segments’ in a fault, defined as those with length of the same order of magnitude as the fault they belong to [*Manighetti et al.*, 2007, 2009], is typically between two and five [*Manighetti et al.*, 2009, 2015], which are subdivided further into smaller ‘secondary’ (or second-order) segments [e.g. *Cartwright et al.*, 1995; *Manighetti et al.*, 2015; *Laó-Dávila et al.*, 2015]. The number of segments appears not to be controlled by fault length, displacement or slip rate [*Manighetti et al.*, 2009, 2015]. Because earthquake magnitude is proportional to rupture area [*Wells and Coppersmith*, 1994], larger earthquakes can occur along interacting fault segments that rupture together, than in single segment ruptures [e.g. *Aki*, 1979; *King and Nabelek*, 1985; *Shen et al.*, 2009]. For segmented faults, interaction between segments influences the maximum coseismic slip magnitude, where slip is underestimated by a single segment length and overestimated from the total fault length [e.g. *Segall and Pollard*, 1980; *Willemsse et al.*, 1996; *Gupta and Scholz*, 2000; *Kase*, 2010]. In addition to altering the maximum rupture length and slip magnitude, interactions between fault segments increase the uncertainty in forecasting earthquakes [*Segall and Pollard*, 1980], as fault segments may rupture individually [e.g. 2004 Parkfield earthquake, *Murray and Segall*, 2002], consecutively [e.g. 1915 Pleasant Valley earthquake, *DePolo et al.*, 1991, 2009 L’Aquila earthquake, *Luccio et al.*, 2010], or continuously in a single event [e.g.

1868 Arica earthquake, Peru, *Bilek and Ruff*, 2002]. Rupture type along a fault may also show temporal variability [e.g. *Bilek and Ruff*, 2002]. Accounting for this uncertainty in maximum or expected earthquake magnitude on a fault is critical for seismic hazard assessments [e.g. *Youngs and Coppersmith*, 1985; *Kijko and Graham*, 1998; *Hodge et al.*, 2015].

One interpretation of how segmented faults form is that initially independent isolated faults undergo interaction and linkage, referred to as the ‘isolated fault model’ [e.g. *Wilcox et al.*, 1973; *Withjack and Jamison*, 1986; *Morley et al.*, 1990; *Trudgill and Cartwright*, 1994; *Cartwright et al.*, 1995; *Dawers and Anders*, 1995]. An alternative theory is that fault segments are already kinematically connected following the inception of a master fault, referred to as the ‘coherent fault model’ [*Walsh et al.*, 2002, 2003]. This hypothesis implies that faults rapidly establish their length, which is followed by a longer phase of slip accumulation without significant fault tip propagation [e.g. *Morewood and Roberts*, 1999; *Nicol et al.*, 2005]. Both isolated and coherent scenarios for fault growth may fit observations within the same region [*Fossen and Rotevatn*, 2016]. Where displacement is transferred between faults or fault segments, but no physical linkage exists, the interacting structures are said to be soft-linked [e.g. *Childs et al.*, 1995; *Kristensen et al.*, 2008]. Hard-linkage is the term used when a physical connection is developed between faults or fault segments. Fault segments may splay from a continuous master fault at depth [*Giba et al.*, 2012], and be geometrically unconnected at the surface for long-periods of time before a hard-linked connection is established [*Walsh et al.*, 2003]. Independent of growth mechanism, hard-links between faults or fault segments develop over time; a question arises of what factors determine the geometrical evolution of this link. Hereafter,

our preference is to use the term ‘fault segment’ to denote the planar structures that a hard-link is established between, but the processes described could also relate to those between ‘isolated’ faults.

Previous studies of fault interaction and linkage have typically focused on strike-slip settings [e.g. *Segall and Pollard*, 1980; *Stein*, 1999; *Chemenda et al.*, 2016], but normal fault systems also show patterns of fault segmentation [*Zhang et al.*, 1991; *Willemse*, 1997; *Giba et al.*, 2012]. Interactions between fault segments can take place through a variety of mechanisms including dynamic coseismic stresses [e.g. *Harris and Day*, 1999; *Duan and Oglesby*, 2005] and driving forces associated with interseismic strain accumulation [e.g. *Peltzer et al.*, 2001; *Dolan et al.*, 2007; *Wedmore et al.*, 2017]. Static coseismic stress changes, associated with fault slip or afterslip, have also been shown to influence interactions between fault segments, and deformation in the area between fault segment tips: the ‘inter-segment zone’ [e.g. *Harris*, 1998; *Stein*, 1999; *Harris and Day*, 1999; *King and Cocco*, 2001; *Duan and Oglesby*, 2005]. In this study, we test the hypothesis that stress changes following one or more earthquakes drive fault linkage by promoting failure on well-oriented secondary faults within the inter-segment zone, here called linking faults. We investigate the role of coseismic stress changes in determining the geometry of hard links, by calculating the permanent stress change on linking faults of fixed orientations. These Coulomb stress changes are derived from the total coseismic slip in an earthquake, or earthquakes, on one or both of the fault segments.

1.1. Hard-Link Development and Geometry

Direct evidence of linkage evolution between fault segments comes from observations of fault geometry using numerical and analogue models [e.g. *Willemse*, 1997; *Aanyu and*

Koehn, 2011; *McBeck et al.*, 2016], and geodetic and seismic studies [e.g. *Taylor et al.*, 2004; *Galli et al.*, 2011; *Long and Imber*, 2012; *Rotevatn and Bastesen*, 2014]. One of the primary influences on initial fault geometry is the regional stress field orientation; in extensional settings, the regional stress supports development of rift-axis parallel, or en echelon, normal faults [e.g. *Ring*, 1994; *Morley*, 1999a]. Tectonic loading then causes elastic stresses that may lead to failure of these faults [e.g. *Cowie and Shipton*, 1998; *Harris and Simpson*, 1996; *Freed*, 2005]. Frictionally weak structures, and/or those with low cohesive strength have, however, been shown to localise deformation and alter the local stress field [e.g. *Ebinger et al.*, 1987; *Bellahsen and Daniel*, 2005; *Collettini et al.*, 2009; *Morley*, 2010]. As segments grow close to one another, stress changes can promote soft-links between fault segments [e.g. *Walsh and Watterson*, 1991; *Childs et al.*, 1995; *Kristensen et al.*, 2008]. A hard-link may then be formed by iterative growth, through fault tip propagation, and intersection between segments [e.g. *McBeck et al.*, 2016], or the failure of well-oriented linking faults within the inter-segment zone [e.g. *Trudgill and Cartwright*, 1994]. Some suggest that soft-links predominantly develop when segments overlap, which then is proceeded by a phase of hard-linkage [e.g. *Acocella et al.*, 2000]. While linking faults may be reactivated pre-existing faults or fractures [e.g. *Bellahsen and Daniel*, 2005; *Collettini et al.*, 2009; *Fagereng*, 2013; *Whipp et al.*, 2014], the stresses at fault segment tips, accumulated over multiple earthquake cycles, can also be sufficient to produce secondary faults and/or fault splays that eventually form the linkage fault zone [e.g. *Bouchon and Streiff*, 1997; *Scholz et al.*, 2010; *Crider*, 2015; *Perrin et al.*, 2016].

The influence of Coulomb stress change on the mechanical interaction between parallel normal faults has been explored before [e.g. *Crider and Pollard*, 1998], but our study

provides an additional step by exploring various linking fault and inter-segment zone geometries between fault segments. We consider three end-member geometrical linking fault configurations: 1) fault bends; 2) breached ramps; and 3) transform faults. Each end-member geometry is outlined below, with reference to natural examples in Table 1 and Figure 1. Although some of the faults in Table 1 comprise more than two segments, we restrict our observations to the hard-link between the two segments with the longest scarp traces. Separation is defined as the strike-perpendicular distance between the tips of the two segments, and overlap as the along-strike distance (where underlap is negative overlap). We define θ as the angle between a line connecting the segment tips and the strike of the segments (where $\theta > 90^\circ$ for overlaps) and α as the acute angle between the strike of a linking fault and that of the fault segments (Figure 2).

1.1.1. Fault Bends

For faults growing in a homogenous, isotropic medium, under a uniformly loaded condition, fault strike should theoretically be constant. Most faults, however, are not perfectly straight, but curve or have abrupt changes in strike, due to interactions with other structures, pre-existing planes of weakness and/or strength anisotropies [e.g. *Faccenna et al.*, 1995; *Acocella et al.*, 2000; *Morley et al.*, 2004; *Fossen and Rotevatn*, 2016]. Fault segments may then establish a hard-link when secondary faults intersect their tips [e.g. *McBeck et al.*, 2016]; where this occurs, the angles θ and α are equivalent. We refer to this type of link as a ‘fault bend’. Examples of fault bends include the 110 km Abadare border fault in the Gregory Rift, East Africa, whose 65 km and 20 km fault segments are linked by a ~ 10 km secondary fault oriented at an angle α of 27° from the average fault segment strike (Figure 1a), and the 25 km Fayette fault in the Wasatch fault zone, Salt

Lake City, whose two ~ 10 km segments are linked by a 4 km secondary fault at an angle α of 39° from the segments [Gawthorpe and Hurst, 1993]. In the range of examples in Table 1, the angle α (and therefore θ) is between 24° and 45° , with an mean of $\sim 30^\circ$ ($n = 6$, Table 1). As the examples were identified from low-resolution maps, the lower limit to α may be significantly less; as it is not always possible to identify and quantify small changes in strike.

1.1.2. Breached Ramps

When fault segments grow towards one another, an elevation gradient called a relay ramp develops between the segments [Larsen, 1988]. Segments separated by relay ramps are initially soft-linked [e.g. Childs et al., 1995; Kristensen et al., 2008]. Hard-linkage occurs when secondary faults begin to nucleate and breach the relay ramp and eventually a through-going fault connects the two fault segments. Relay ramp hard-linkages are distinguishable from fault bends as their segment tips extend along-strike beyond the point of hard-linked connection [e.g. Trudgill and Cartwright, 1994, Figure 1b]. Examples include a ~ 20 km section of the Parihaka Fault, New Zealand [Giba et al., 2012] formed of two ~ 10 km segments, and the Deer Fault, USA [Commins et al., 2005], a small, segmented, 1 km long fault, both oriented at an angle $\alpha \sim 34^\circ$ from the strike of the fault segments (Figure 1b). All examples have a $\theta > 90^\circ$, and the angle α is between 24° and 74° , with an mean of $\sim 45^\circ$ ($n = 8$, Table 1).

1.1.3. Transform Faults

The term transform fault has been used to describe strike-slip linking structures at various scales [Morley et al., 1990; Peacock and Sanderson, 1994; Trudgill and Cartwright, 1994]. Here, transform faults are defined as sub-vertical structures, with a significant

component of strike-slip displacement. While transform faults are common at mid-ocean ridge settings, examples of continental transforms linking normal faults are rare. Within the Rio Grande Rift, USA, 30 km to 40 km long fault segments are linked through transform faults oriented $\alpha \sim 75^\circ$ from the fault segments [Gawthorpe and Hurst, 1993; Faulds and Varga, 1998]. In the Rusizi Rift, East Africa, a transform fault zone links normal fault segments at an angle α of $\sim 87^\circ$, where θ is 100° (Figure 1c). The angle α is found to be between 60° and 90° , with an mean of $\sim 75^\circ$ ($n = 6$, Table 1).

2. Methods

2.1. Coulomb Stress Change

Coulomb stress change ($\Delta\sigma_c$) is the change in static stress state caused by slip on a source fault, resolved onto a receiver fault. It is defined by the following equation:

$$\Delta\sigma_c = \Delta\tau_s - \mu' \Delta\sigma_n \quad (1)$$

where $\Delta\tau_s$ is the shear stress change (positive in the inferred slip direction), $\Delta\sigma_n$ is the normal stress change (negative when the fault is unclamped) and μ the static friction coefficient. The effect of pore pressure p can be related to confining stress by Skempton's coefficient β , which typically has a value between 0 and 1. Pore pressure, p , is included through the effective friction coefficient, $\mu' = \mu(1 - \beta)$, where $\beta = p/\sigma_n$. Thus, an increase in pore pressure will increase the Coulomb stress and bring a fault closer to failure.

Within static Coulomb stress change models, processes such as dynamic clamping or unclamping are not included [e.g. Freed, 2005; Toda *et al.*, 2011], even though dynamic stresses produce larger, transient stress change magnitudes [Gomberg *et al.*, 1998; Stein,

1999]. Static Coulomb stress change models have, however, been shown to successfully model the distribution of aftershocks and provide a tool for forecasting earthquake sequences [e.g. *Harris and Simpson, 1992; Hill et al., 1995; Gomberg, 1996; Stein et al., 1997; Ziv and Rubin, 2000; Lin and Stein, 2004; Wedmore et al., 2017*]. Coulomb stress change may either increase or decrease the time to the next failure on a fault [*King et al., 1994*]; positive values are said to promote failure (clock advance) and negative values retard failure, where a positive $\Delta\sigma_c$ is associated with earthquake triggering at distances of a few fault lengths [e.g. *Harris, 1998; Stein, 1999; King and Cocco, 2001; Nicol et al., 2010*]. Increasing the Coulomb stress on a fault is not in itself enough to generate failure as it is also important whether the fault is already close to failure. Previous studies suggest a $\Delta\sigma_c$ of 0.1 MPa is sufficient to generate aftershocks on a range of nearby faults [e.g. *King et al., 1994; Lin and Stein, 2004*]; but the precise value is sensitive to a range of factors [e.g. *King et al., 1994; Gomberg, 2001*].

We used Coulomb 3.4 [*Toda et al., 2011*], a homogenous elastic half-space model based on *Okada [1992]*, to investigate the coseismic Coulomb stress changes around a normal source fault, on evenly spaced receiver faults. Source fault earthquake parameters were kept constant and related to an earthquake of $\sim M_W$ 6.5 (M_o 5.5×10^{22} Nm) on an Andersonian normal fault with strike = 0° , dip = 60° W, rupture length $l = 20$ km, rupture width $w = 17$ km, fault top depth = 0 km, fault bottom depth = 15 km, and uniform slip $u = 1$ m. Although slip to rupture length ratios can vary considerably [e.g. *Wells and Coppersmith, 1994*], we use a slip to rupture length ratio of 5×10^{-5} [*Walsh et al., 2002*], a value in the middle of global extrema [*Shaw and Scholz, 2001*]. Receiver fault strike, dip and slip vector rake (vector which shear stress is resolved along) are fixed

for each model but varied systematically to explore end-member linking fault geometries.

We do not apply any background stresses; in essence, we study the static stress change of an earthquake, or earthquakes, on a particular receiver fault geometry. The concept of tectonic loading is discussed later. A grid size of 1 x 1 km was chosen for receiver fault calculations as this was found to be optimal for resolution and processing times.

The effect of Poisson's ratio, ν , on $\Delta\sigma_c$ is negligible, and therefore we set ν to the default 0.25 as used in previous Coulomb stress change studies [e.g. *Willemsse, 1997; Crider and Pollard, 1998; Zhao et al., 2004*]. For Young's modulus E we use an upper to mid crustal value of 60 GPa [*Bilham et al., 1995; Zhao et al., 2004*], and set the effective friction coefficient μ' to 0.4, a value suitable for large continental faults [*Harris, 1998*]. In our sensitivity tests we run our model using a range of μ' values, including larger values that are more appropriate to the development of new secondary faults [e.g. *Byerlee, 1978*], and smaller values associated with weak zones where reactivation of pre-existing structures may occur [e.g. *Collettini et al., 2009*].

2.2. Model Setup

In order to compare coseismic Coulomb stress changes for a number of linking fault configurations and distances between parallel normal fault segments, we simplify the geometry of the source fault(s), inter-segment zone and receiver faults. Source faults mimic the active fault segments and are modelled as planar, with constant strike, as illustrated in Figure 1. As inter-segment zones are densely faulted and fractured [e.g. *Anders and Wiltschko, 1994; Faulkner et al., 2011*], we assume there will be a fracture surface available in any geometry and consider only a single receiver fault in the centre of the zone, which denotes the linking fault (Figure 3c). We consider two scenarios: the 'single seg-

ment rupture scenario', in which an earthquake rupturing only one fault segment changes the Coulomb stress on a linking fault; and the 'two segment rupture scenario', where two earthquakes, or a single earthquake propagating across the geometrical discontinuity, rupture(s) both fault segments. We vary the along-strike distance between fault segments from 10 km underlap to 4 km overlap in 2 km increments, and the fault separation from 2 km to 10 km in 2 km increments (Figure 3). Table 2 shows the geometries for the three end-member linking fault configurations: 1) fault bend; 2) breached ramp; and 3) transform faults.

We also consider whether at certain inter-segment zone geometries continued growth of fault segments without a change in strike is preferred to our linkage configurations ('Along-strike', Table 2). This scenario is analysed by calculating $\Delta\sigma_c$ on a receiver fault located along-strike from the fault segment, hereafter called the 'along-strike secondary fault'. If the $\Delta\sigma_c$ magnitude of this along-strike secondary fault is larger than all linking fault configurations, we determine this growth scenario to be preferred. The receiver fault is located at half the along-strike distance between the fault segments (marked G, Figure 3c), except where it falls within one grid space of the fault segment, in which case an along-strike distance of 2 km from the segment tip is used instead.

3. Results

3.1. Numerical Models

Figure 4a shows the coseismic Coulomb stress changes between an echelon fault segments, for our three end-member linking fault geometries, using the single segment rupture scenario. For fault bends and breached ramps, $\Delta\sigma_c$ is positive for all underlapping inter-segment zone geometries and negative for all overlapping geometries. In both cases,

the magnitude decreases with increasing separation. In contrast, for transform faults, $\Delta\sigma_c$ is positive for large values of separation and negative for small values when segments are underlapping, and $\Delta\sigma_c$ is positive for all overlapping geometries. The preferred link geometry, that with the largest $\Delta\sigma_c$ magnitude, is presented in Figure 4b for all values of overlap/underlap and separation. Fault bends are preferred in underlapping geometries when the amount of separation is equal to, or less, than the underlap ($\theta \leq 45^\circ$). Breached ramps are preferred only in underlapping geometries when separation is greater than underlap ($\theta > 45^\circ$). Transform faults are preferred when the segments overlap.

In general the two segment rupture scenario produces larger magnitude $\Delta\sigma_c$ compared to the single segment rupture scenario (Figure 5a). For fault bends and breached ramps, the exceptions are where $O \geq 0$ km, in which case $\Delta\sigma_c$ is slightly larger for the single segment rupture scenario for large values of separation (Figure 4a). This is because fault bends and ramps are unfavourable geometries for linking overlapping faults, so that $\Delta\sigma_c$ is negative for a single rupture, and becomes more negative in the two rupture scenario. The only difference in preferred link geometry occurs at separations of 8 km to 10 km when underlap is 2 km, where transform faults are preferred to breached ramps using the two segment rupture scenario (Figure 5b).

We now compare the $\Delta\sigma_c$ of the preferred linking fault geometry to the $\Delta\sigma_c$ of the along-strike secondary fault for each inter-segment zone geometry (Figure 6). For the single segment rupture scenario, along-strike secondary faults have a larger Coulomb stress magnitude for most cases, except for separations of 2 km, where linkage of en echelon fault segments through transform faults are preferred when $O = 0$ km, and faults bends or breached ramps at an underlap of 2 km (Figure 6a). For the two segment rupture scenario,

along-strike secondary faults are not as dominant but are always favoured if separation is greater than 8 km (Figure 6b). Where fault bends were the favoured link geometry without considering along-strike secondary faults, they are still preferred over along-strike secondary faults, i.e. they have a larger Coulomb stress magnitude. Transform faults are still preferred for $O \geq 0$ km providing the separation is less than 8 km. Where breached ramps were the favoured linking geometry, along-strike secondary faults are now favoured in all cases except for those of low underlap and separation 4 km or less.

3.2. Sensitivity Tests

The numerical modelling uses simplified end-member fault geometries and slip distributions, thus we test the sensitivity of our results to the model assumptions, including: 1) slip distribution on, and between, fault segments; 2) linking fault geometry; 3) linking fault location; and 4) calculation depth (supplementary material). Applying a different magnitude of slip on each fault segment, or applying a tapered rather than uniform slip distribution along the segments [e.g. *Cowie and Scholz, 1992a; Schultz et al., 2008; Wesnousky, 2008; Perrin et al., 2016*], does not change the preferred link geometry in the majority of cases (Figures S3-5). More complex slip distributions may, however, influence link geometry through modification of the stress distribution within the inter-segment zone [e.g. *Noda et al., 2013*]. Further details of the limited number of exceptions are given in the supplementary material. Similarly, we find that the same link geometry is preferred regardless of the calculation depth, since although the absolute values of $\Delta\sigma_c$ change, the relative values do not. In addition, we changed the effective friction coefficient from 0.4 to 0.2 and 0.6 to reflect hard-links establishing in strong or weak zones, respectively. This

change increased, or decreased, $\Delta\sigma_c$ by less than 1 MPa, respectively, but had no effect on the preferred link geometry.

We fix the linking fault geometry to simplified end-member configurations, so we test whether an alternative orientation would experience larger Coulomb stress change, using three representative examples, one for each end-member link style (Figure 7a-c). For geometries where end-member fault bend and breached ramp configurations were preferred, a greater $\Delta\sigma_c$ magnitude occurs on linking faults striking with a slightly lower angle to the fault segment strike, with a steeper dip and small left-lateral component of slip (Figure 7a,b). For a geometry where our end-member transform fault configuration (Figure 7c) was preferred, a greater $\Delta\sigma_c$ magnitude occurs on linking faults with shallower dip and significant normal component. This is consistent with studies on faults in the Gulf of Suez, which show that secondary faults with an oblique sense of slip and a larger normal component form hard-links between normal fault segments [McClay and Khalil, 1998].

Furthermore, by fixing the location of the linking fault within the inter-segment zone, we neglect the possibility that linking faults form off-centre. In particular, there is evidence that through-going secondary faults preferentially breach the base of relay ramps, rather than at the crest [e.g. Crider and Pollard, 1998; Crider, 2001; Peacock, 2002; Soliva and Benedicto, 2004; Commins et al., 2005; Fossen and Rotevatn, 2016]. Sensitivity tests for a range of locations within a relay ramp show that the largest $\Delta\sigma_c$ occurs closer to the fault segment tip at the upper or lower end of the relay ramp (Figure S7). Importantly, the $\Delta\sigma_c$ at the upper and lower end of relay ramps does in some cases exceed that of other, otherwise preferred linkage geometries (Figure 7d). In the further discussion, we

use the breached relay ramp linking fault with greatest $\Delta\sigma_c$ at any location within the inter-segment zone.

3.3. Comparison to Observations

To test the hypothesis that the stress field in the inter-segment zone is dominated by coseismic Coulomb stress changes and hence shapes the geometry of the hard-link between fault segments, we compare our model results to observations of normal fault surface trace geometry (Table 1). In Figure 8a we plot the observations alongside the two segment rupture scenario results. We extend our model to include inter-segment zone geometries up to 10 km overlap; observations outside the model space are shown by an arrow. As fault and segment lengths varied over an order of magnitude among observations, we normalised overlap and separation to compare with model results. For model results, segment separation and overlap were normalised to the total length of the segments used in this study (40 km). For observations, we normalised to the total length of the two hard-linked segments (Table 1). The natural observations of hard-links between fault segments are recorded at the surface, whereas our model results are taken from a calculation depth of 10 km. However, we found that link type does not vary with calculation depth (Figure S9). Furthermore, as our observations come from similar tectonic settings, we assumed all other fault parameters are the within the same magnitude as used in this study. The slip to length ratio may show variation between observations [e.g. *Scholz*, 2002], but this would only change the absolute $\Delta\sigma_c$ magnitude, not the relative magnitude between linking configurations that is pertinent here.

All fourteen fault bend and breached ramp observations match model results (Figure 8a). No fault bend or breached ramp observations fell within regions predicted by

the model to favour along-strike secondary faults, suggesting there is a maximum inter-segment zone geometry hard-links do not occur beyond. Half of observations of transform faults, three out of six, fell within model predictions for breached ramp linking faults: The Rusizi Rift (17), North Craven and Middle Craven (19) and Central Betics Fault Zone (20) transform faults. The Gulf of Evvia (15) and Bare Mountain Fault Zone (16) transform faults are within one model grid space. However, our model predicts a preference of along-strike secondary faults for the majority of transform observations (five out of six), even those that fall within breached ramp regimes in underlapping geometries.

Observations of normal faults and surface ruptures show linkage and rupture propagation between segments separated up to 10 km [Table 1; *Biasi and Wesnousky, 2016*]. In our model, for two 20 km fault segments, coseismic Coulomb stress change magnitude was larger on along-strike secondary faults than linking faults for fault segments separated by distances of 8 km or greater (Figure 8a). Using data from *Biasi and Wesnousky [2016]*, and results from this study, a correlation between maximum separation and total length of segments is found (Figure 8b). Here, empirically, it appears that the maximum step distance does not exceed 20% the total length of the interacting segments. Only two transform faults from our twenty natural observations of hard-linkage had a larger separation. Small intermediate fault segments within the inter-segment zone may also hinder hard-linkage at the largest separations, by perturbing rupture propagation across the inter-segment zone [e.g. *Lozos et al., 2012, 2015*]. Assuming constant stress drop, the empirical scaling between maximum separation and total fault segment length arises from that stress intensity at the fracture tip increases with fault length [*Rudnicki, 1980; Segall and Pollard, 1980*]. This relationship from linear elastic fracture mechanics implies that

fault linkage is promoted in the zone between en echelon cracks, in a zone which shape depends on slip sense, and which size increases with fault length [Segall and Pollard, 1980; Cowie and Scholz, 1992b].

4. Discussion

4.1. Hard-Link Development and Geometry

The comparison between natural observations and our model results (Figure 8a) is consistent with the concept that the type of hard-link is influenced by the inter-segment zone geometry. Contrary to previous studies that suggest that hard-links establish in overlapping regimes [e.g. Acocella *et al.*, 2000], our results suggest that linkage may also develop in underlapping geometries through breached relay ramps, but predominantly as fault bends. Coulomb stress change calculations may also estimate whether continued along-strike growth of segments, through links with along-strike secondary faults, is preferred to hard-linkage between parallel fault segments; however, we are unable to compare our results to real-world examples because along-strike growth or linkage does not produce a change in strike, so cannot be easily identified in the geomorphology.

Continental transform faults are rarely observed linking normal fault segments in nature, and those that we could find evidence for occurred over a wide range of fault geometries (Table 1). There are a number of explanations for why our models do not match observations for transform faults. A possibility is that coseismic Coulomb stress changes could promote the establishment of hard-links before fault segments reach the geometrically preferred criteria for transform faults, i.e. through fault bends or breached relay ramps at underlapping geometries, or segments may continue to grow along-strike if separation is large (Figure 6). Even when fault segments reach the preferred geometry for transform

faults, Coulomb stress change magnitude is larger on high-angle linking faults that have a dip-slip component (Figure 7); therefore, transform faults that were previously thought to be strike-slip, may in fact involve a significant dip-slip motion [e.g. *McClay and Khalil, 1998*].

Our results indicate that when only one fault segment ruptures, continued along-strike growth of segments is preferred (Figure 4). Discrete earthquakes on two parallel segments, or a single earthquake whose rupture propagates across the inter-segment zone, favours the promotion of a hard-link between offset segments (Figure 5). Earthquakes that rupture multiple faults or fault segments such as Landers 1992 M_W 7.3 [*Sieh et al., 1993*], Wenchuan 2008 M_W 7.9 [*Shen et al., 2009*], Haiti 2010 M_W 7.0 [*Hayes et al., 2010; De Lépinay et al., 2011*] and Kaikoura 2016 M_W 7.8 [*Hamling et al., 2017*], or earthquake sequences such as Friuli 1976 sequence [*Cipar, 1980*], the Umbria-Marche 1997 sequence [*Amato et al., 1998*], Karonga 2009 sequence [*Biggs et al., 2010*] and the Amatrice-Norcia 2016 sequence [*Cheloni et al., 2017*], therefore promote the development of hard-links. Furthermore, Coulomb stress changes in regions with dense fault networks can cause periods of increased seismic activity [e.g. *Wedmore et al., 2017*], increasing the frequency of interactions between faults segments, and thus, the potential for hard-linkages to establish. The geometry of the inter-segment zone at the time of a multi-segment rupture, or earthquake sequence, then influences the geometry of the hard-link. For example, segments with small amounts of separation may link through fault bends if a multi-segment rupture or earthquake sequence occurs during the underlapping phase, whereas consecutive single segment ruptures may promote continued along-strike growth to overlapping inter-segment zone geometries, where breached ramps are then preferred (Figure 4). How-

ever, this ultimately depends on the time between coseismic events on the segments and surrounding ruptures that may cause stress shadows within the inter-segment zone [e.g. *Stein, 1999*].

If segment growth and linkage is considered to occur via the isolated fault model [e.g. *Morley et al., 1990; Trudgill and Cartwright, 1994; Cartwright et al., 1995; Dawers and Anders, 1995*], rupture propagation across inter-segment zones and/or earthquake interaction between fault segments is required [e.g. *Harris and Day, 1993, 1999; Kilb et al., 2000; Gomberg et al., 2001*]. The coherent fault model assumes kinematic connectivity, and thus soft-links at depth exists already, promoting the two segment rupture scenario through a continuous rupture [*Walsh et al., 2002, 2003*]. Whether a rupture propagates through the inter-segment zone in either model depends on the zone's mechanical properties, which are related to certain fault properties such as slip maturity [e.g. *Ikari et al., 2011; Savage and Brodsky, 2011*].

Similar to previous models that sought to understand growth processes occurring at fault tips following an earthquake, an assumption made here is that coseismic stress perturbations exceed the stresses from tectonic loading [e.g. *Cowie and Shipton, 1998*]. Ignoring tectonic loading allows us to examine the influence of coseismic Coloumb stress change on linking fault geometry without the complicating effect of faults nucleating due to background stresses [*Fialko, 2006*]. However, tectonic loading may cause slip on secondary faults that are poorly oriented for segment linkage but well-oriented for reshear in the tectonically induced stress field [*Harris and Simpson, 1996; Freed, 2005*]. Formation of new faults controlled by tectonic loading is also likely if the segment separation is large and off-fault deformation accommodates slip transfer between segments [*Duan and*

Oglesby, 2005]. Tectonic loading may therefore promote along-strike growth of segments that are well-oriented in the current stress field, and favour hard-links between overlapping segments whose tips propagate into a stress shadow [e.g. Harris, 1998; Lin and Stein, 2004; Ganas *et al.*, 2006].

Dynamic coseismic, interseismic or multi-cycle effects likely further influence fault linkage [e.g. Harris, 1998; Kase, 2010] and may also cause failure of faults with geometries that are deemed retarded by Coulomb stress models [e.g. Kilb *et al.*, 2000; Gomberg *et al.*, 2001]. Multi-cycle effects include increasing fault zone structural maturity, which reduces the strength of the inter-segment zone between fault segments [e.g. Wesnousky, 1988; Otsuki and Dilov, 2005] and can cause interaction and rupture propagation to occur over larger fault lengths, including several segments [e.g. Manighetti *et al.*, 2007], and changes to the frictional strength of fault surfaces due to the grinding away of asperities [Sagy *et al.*, 2007]. Furthermore, multiple earthquake cycles will also increase the stress concentration at fault tips [e.g. Pollard and Segall, 1987; Cowie and Scholz, 1992a] and thus within the inter-segment zone.

Linking faults may establish through incremental earthquake rupture and associated damage around the fault tip [Herbert *et al.*, 2015; McBeck *et al.*, 2016]. Fault segments where $\theta < 30^\circ$ may propagate toward one another, whereas at higher angles new oblique-slip secondary faults may develop to form a relay ramp hard-link [Hatem *et al.*, 2015]. Our model results show that fault bends form up to a θ of 45° , however, the majority of our natural observations for fault bends had a $\theta < 30^\circ$. Analogue models have shown that pre-existing structures may provide a pathway for fault bends to establish when θ is between 30° and 45° [e.g. Morley *et al.*, 2004].

4.2. The Influence of Pre-existing Structures

The geometry and development of normal faults is primarily influenced by the regional and local stress fields [e.g. *Ring, 1994; Morley, 1999b*]. However, in this study we have shown how coseismic Coulomb stress changes influence the geometry of a hard-link between en echelon faults by altering the local stress field [Figure 8; e.g. *Harris and Simpson, 1992; King et al., 1994; Crider and Pollard, 1998*]. Pre-existing structures that have a lower cohesive or frictional strength than the surrounding intact rock have been shown to localise deformation and alter the local stress field [e.g. *Ebinger et al., 1987; Bellahsen and Daniel, 2005; Collettini et al., 2009*], and therefore may also influence the establishment and geometry of the hard-link [e.g. *Rosendahl, 1987; Lezzar et al., 2002; Morley et al., 2004; Corti et al., 2007; Bellahsen et al., 2013; Reeve et al., 2015*] by reducing the required $\Delta\sigma_c$ for failure. Here, we provide conceptual examples of pre-existing weak planes striking at various angles to normal faults, with an extension vector E-W (Figure 9).

When weak pre-existing structures strike parallel to the faults (Figure 9a), fault linkage is likely perturbed until faults overlap and cannot propagate further at their tips due to stress shadows [e.g. *Harris, 1998; Lin and Stein, 2004; Ganas et al., 2006*], at which point a hard-link can only establish by cross-cutting the pre-existing fabric. Rift-parallel pre-existing crustal weaknesses around Lake Albert, East Africa have helped formed overlapping, en echelon normal faults arrays [*Aanyu and Koehn, 2011*] and may therefore help faults develop the inter-segment geometry required for breached ramps or continental transform faults [e.g. *Rosendahl, 1987; Bellahsen et al., 2013*]. If the strike of pre-existing structures are well-oriented for fault linkage (i.e. at angle θ to the fault segments), but oblique to the extension direction (Figure 9b, right-stepping), fault bends or breached

ramps may be promoted during underlapping and overlapping geometries, respectively, if the pre-existing structure is sufficiently weak compared to along-strike structures. Several examples of hard-linkages along border faults in Lake Tanganyika have been shown to exploit well-oriented, pre-existing planes of weakness [e.g. *Lezzar et al.*, 2002; *Corti et al.*, 2007]. Lastly, hard-links are promoted if pre-existing structures are favoured by the regional stress orientation and have a strike close to θ , however, this requires a stress rotation from a regional stress orientation that formerly favoured the geometry of the en echelon faults (Figure 9c, left-stepping). Conversely, weak pre-existing structures may inhibit fault linkage by providing surfaces for failure that are poorly-oriented for fault linkage.

5. Conclusion

In this paper we have discussed the role of coseismic Coulomb stress change on shaping the hard-link between two en echelon normal fault segments (or faults). Coulomb stress changes can promote failure on a well-oriented secondary fault, a linking fault, incrementally forming a hard-link between segments. Linking faults may nucleate within the inter-segment damage zone, or reactivate pre-existing structures. Our calculations indicate that the two segments must both rupture for the greatest stress change to occur on a linking fault within the inter-segment zone, rather than on a segment-parallel secondary fault aligned along strike from the segment tip. This may occur either through the aggregate effect of discrete events on both segments (i.e. an earthquake sequence), or as a single earthquake whose rupture propagates across the geometrical discontinuity (i.e. a multi-segment rupture). When only one segment ruptures, the Coulomb stress

change is largest for the along-strike secondary fault, and thus continued segment growth is preferred at all geometries except very close to the segment tips.

Our results match well with natural examples of hard-links between normal fault segments, and show that the linking fault geometry that experiences the greatest coseismic Coulomb stress change is related to the geometry of the inter-segment zone. Here, we suggest that underlapping parallel normal segments preferentially link through fault bends or breached ramps when separation is $\leq 20\%$ of the total length of both segments, and $\theta \leq 45^\circ$ or $\theta > 45^\circ$, respectively. Fault segments that grow to overlapping geometries preferentially link through either transform faults when separation is $\gtrsim 15\%$ of the total length, or breached ramps at smaller separations. Maximum separation for segment hard-linkage was found to be $\sim 20\%$ the total segment lengths, agreeing with previous studies of normal fault surface rupture traces. At larger separations the coseismic Coulomb stress change is largest for along-strike secondary faults.

Whilst natural examples of hard-links between normal fault segments through fault bends and breached ramps are plentiful, the same is not true for continental transform faults. An explanation from this study is that normal fault segments may link through fault bends or breached ramps in underlapping regimes before they reach the geometries required for transform faults.

Acknowledgments. The data used are listed in the references, tables, and supplements. MH is supported by the NERC GW4+ Doctoral Training Partnership (grant code NE/L002434/1), and Centre for Observation and Modelling of Earthquakes, Volcanoes and Tectonics (COMET). JB is supported by COMET and a NERC large grant “Looking Inside the Continents from Space (LICS)” (grant code NE/K010913/1). We thank

the editors and anonymous reviewers for their constructive comments, which have greatly helped improve the quality of the manuscript.

Accepted Article

References

- Aanyu, K., and D. Koehn (2011), Influence of pre-existing fabrics on fault kinematics and rift geometry of interacting segments: Analogue models based on the Albertine Rift (Uganda), Western Branch-East African Rift System, *Journal of African Earth Sciences*, *59*(2-3), 168–184, doi:10.1016/j.jafrearsci.2010.10.003.
- Acocella, V., F. Salvini, R. Funiciello, and C. Faccenna (1999), The role of transfer structures on volcanic activity at Campi Flegrei (Southern Italy), *Journal of Volcanology and Geothermal Research*, *91*(2-4), 123–139, doi:10.1016/S0377-0273(99)00032-3.
- Acocella, V., A. Gudmundsson, and R. Funiciello (2000), Interaction and linkage of extension fractures and normal faults: Examples from the rift zone of Iceland, *Journal of Structural Geology*, *22*(9), 1233–1246, doi:10.1016/S0191-8141(00)00031-6.
- Aki, K. (1979), Characterization of barriers on an earthquake fault, *Journal of Geophysical Research*, *84*(B11), 6140, doi:10.1029/JB084iB11p06140.
- Aldrich, M. J., C. E. Chapin, and A. W. Laughlin (1986), Stress History and Tectonic Development of the Rio Grande Rift, New Mexico, *Journal of Geodynamics*, *91*(4), 6199–6211.
- Amato, A., R. Azzara, C. Chiarabba, G. Cimini, M. Cocco, M. Di Bona, L. Margheriti, S. Mazza, F. Mele, G. Selvaggi, A. Basili, and E. Boschi (1998), The 1997 Umbria-Marche, Italy, earthquake sequence: a first look at the main shocks and aftershocks, *Geophysical Research Letters*, *25*(15), 2861–2864.
- Anders, M. H., and D. V. Wiltschko (1994), Microfracturing, paleostress and the growth of faults, *Journal of Structural Geology*, *16*(6), 795–815.

Bellahsen, N., and J. M. Daniel (2005), Fault reactivation control on normal fault growth: an experimental study, *Journal of Structural Geology*, *27*(4), 769–780, doi:10.1016/j.jsg.2004.12.003.

Bellahsen, N., S. Leroy, J. Autin, P. Razin, E. D’Acremont, H. Sloan, R. Pik, A. Ahmed, and K. Khanbari (2013), Pre-existing oblique transfer zones and transfer/transform relationships in continental margins: New insights from the southeastern Gulf of Aden, Socotra Island, Yemen, *Tectonophysics*, *607*, 32–50, doi:10.1016/j.tecto.2013.07.036.

Biasi, G. P., and S. G. Wesnousky (2016), Steps and Gaps in Ground Ruptures: Empirical Bounds on Rupture Propagation, *Bulletin of the Seismological Society of America*, *106*(3), 1110–1124, doi:10.1785/0120150175.

Biggs, J., E. Nissen, T. Craig, J. Jackson, and D. P. Robinson (2010), Breaking up the hanging wall of a rift-border fault: The 2009 Karonga earthquakes, Malawi, *Geophysical Research Letters*, *37*(11), doi:10.1029/2010GL043179.

Bilek, S. L., and L. J. Ruff (2002), Analysis of the 23 June 2001 $M_w = 8.4$ Peru underthrusting earthquake and its aftershocks, *Geophysical Research Letters*, *29*(20), 21–21–4, doi:10.1029/2002GL015543.

Bilham, R., P. Bodin, and M. Jackson (1995), Entertaining a great earthquake in western Nepal: Historic inactivity and geodetic tests for the present state of strain, *Journal of Nepal Geological Society*, *11*(1), 73–78.

Bouchon, M., and D. Streiff (1997), Propagation of a Shear Crack on a Nonplanar Fault: A Method of Calculation, *Bulletin of the Seismological Society of America*, *87*(1), 61–66.

Byerlee, J. (1978), Friction of rocks, *Pure and applied Geophysics*, *116*(4), 615–626.

Cartwright, J. A., B. D. Trudgill, and C. S. Mansfield (1995), Fault growth by segment linkage: an explanation for scatter in maximum displacement and trace length data from the Canyonlands Grabens of SE Utah, *Journal of Structural Geology*, *17*(9), 1319–1326, doi:10.1016/0191-8141(95)00033-A.

Cheloni, D., V. De Novellis, M. Albano, A. Antonioli, M. Anzidei, S. Atzori, A. Avallone, C. Bignami, M. Bonano, S. Calcaterra, R. Castaldo, F. Casu, G. Cecere, C. De Luca, R. Devoti, D. Di Bucci, A. Esposito, A. Galvani, P. Gambino, R. Giuliani, R. Lanari, M. Manunta, M. Manzo, M. Mattone, A. Montuori, A. Pepe, S. Pepe, G. Pezzo, G. Pietrantonio, M. Polcari, F. Riguzzi, S. Salvi, V. Sepe, E. Serpelloni, G. Solaro, S. Stramondo, P. Tizzani, C. Tolomei, E. Trasatti, E. Valerio, I. Zinno, and C. Doglioni (2017), Geodetic model of the 2016 Central Italy earthquake sequence inferred from InSAR and GPS data, *Geophysical Research Letters*, *44*(13), 6778–6787, doi:10.1002/2017GL073580.

Chemenda, A. I., O. Cavalié, M. Vergnolle, S. Bouissou, and B. Delouis (2016), Numerical model of formation of a 3-D strike-slip fault system, *Comptes Rendus Geoscience*, *348*(1), 61–69, doi:10.1016/j.crte.2015.09.008.

Childs, C., J. Watterson, and J. J. Walsh (1995), Fault overlap zones within developing normal fault systems, *Journal - Geological Society (London)*, *152*(3), 535–549, doi:10.1144/gsjgs.152.3.0535.

Cipar, J. (1980), Teleseismic observations of the 1976 Friuli, Italy earthquake sequence, *Bulletin of the Seismological Society of America*, *70*(4), 963–983.

Collettini, C., A. Niemeijer, C. Viti, and C. Marone (2009), Fault zone fabric and fault weakness., *Nature*, *462*(7275), 907–10, doi:10.1038/nature08585.

Commins, D., S. Gupta, and J. A. Cartwright (2005), Deformed streams reveal growth and linkage of a normal fault array in the Canyonlands graben, Utah, *Geology*, *33*(8), 645–648, doi:10.1130/G21433.1.

Corti, G., J. van Wijk, S. Cloetingh, and C. K. Morley (2007), Tectonic inheritance and continental rift architecture: Numerical and analogue models of the East African Rift system, *Tectonics*, *26*(6), 1–13, doi:10.1029/2006TC002086.

Cowie, P. a., and C. H. Scholz (1992a), Growth of faults by accumulation of seismic slip, *Journal of Geophysical Research*, *97*(B7), 11,085, doi:10.1029/92JB00586.

Cowie, P. A., and C. H. Scholz (1992b), Physical Explanation for the Displacement Length Relationship of Faults Using a Post-Yield Fracture-Mechanics Model, *Journal of Structural Geology*, *14*(10), 1133–1148, doi:10.1016/0191-8141(92)90065-5.

Cowie, P. A., and Z. K. Shipton (1998), Fault tip displacement gradients and process zone dimensions, *Journal of Structural Geology*, *20*(8), 983–997, doi:10.1016/S0191-8141(98)00029-7.

Crider, J. G. (2001), Oblique slip and the geometry of normal-fault linkage: Mechanics and a case study from the Basin and Range in Oregon, *Journal of Structural Geology*, *23*(12), 1997–2009, doi:10.1016/S0191-8141(01)00047-5.

Crider, J. G. (2015), The initiation of brittle faults in crystalline rock, *Journal of Structural Geology*, *77*, 159–174, doi:10.1016/j.jsg.2015.05.001.

Crider, J. G., and D. D. Pollard (1998), Fault linkage : Three-dimensional mechanical interaction faults, *Journal of Geophysical Research*, *103*(B10), 24,373–24,391.

Dawers, H., and M. H. Anders (1995), Displacement-length scaling and fault linkage, *Journal of Structural Geology*, *17*(5), 607–614.

De Lépinay, B. M., A. Deschamps, F. Klingelhoefer, Y. Mazabraud, B. Delouis, V. Clouard, Y. Hello, J. Crozon, B. Marcaillou, D. Graindorge, M. Vallée, J. Perrot, M. P. Bouin, J. M. Saurel, P. Charvis, and M. St-Louis (2011), The 2010 Haiti earthquake: A complex fault pattern constrained by seismologic and tectonic observations, *Geophysical Research Letters*, *38*(22), 1–7, doi:10.1029/2011GL049799.

DePolo, C. M., D. G. Clark, D. Slemmons, and A. R. Ramelli (1991), Historical surface faulting in the Basin and Range province, western North America: implications for fault segmentation, *Journal of Structural Geology*, *13*(2), 123–136, doi: [http://dx.doi.org/10.1016/0191-8141\(91\)90061-M](http://dx.doi.org/10.1016/0191-8141(91)90061-M).

Dolan, J. F., D. D. Bowman, and C. G. Sammis (2007), Long-range and long-term fault interactions in Southern California, *Geology*, *35*(9), 855–858, doi:10.1130/G23789A.1.

Duan, B., and D. D. Oglesby (2005), Multicycle dynamics of nonplanar strike-slip faults, *Journal of Geophysical Research*, *110*, 1–16, doi:10.1029/2004JB003298.

Duffy, O. B., S. H. Brocklehurst, R. L. Gawthorpe, M. R. Leeder, and E. Finch (2014), Controls on landscape and drainage evolution in regions of distributed normal faulting: Perachora Peninsula, Corinth Rift, Central Greece, *Basin Research*, pp. 473–494, doi: 10.1111/bre.12084.

Ebinger, C., B. Rosendahl, and D. Reynolds (1987), Tectonic model of the Malawi rift, Africa, *Tectonophysics*, *141*, 215–235.

Faccenna, C., T. Nalpas, J.-P. Brun, P. Davy, and V. Bosi (1995), The influence of pre-existing thrust faults on normal fault geometry in nature and in experiments, *Journal*

of *Structural Geology*, 17(8), 1139–1149, doi:10.1016/0191-8141(95)00008-2.

Fagereng, Å. (2013), Fault segmentation, deep rift earthquakes and crustal rheology: Insights from the 2009 Karonga sequence and seismicity in the Rukwa-Malawi rift zone,

Tectonophysics, 601(December 2009), 216–225, doi:10.1016/j.tecto.2013.05.012.

Faulds, J. E., and R. J. Varga (1998), The role of accommodation zones and transfer zones in the regional segmentation of extended terranes, *Geological Society of America*

Special Papers, 323, 1–45, doi:10.1130/0-8137-2323-X.1.

Faulkner, D. R., T. M. Mitchell, E. Jensen, and J. Cembrano (2011), Scaling of fault damage zones with displacement and the implications for fault growth processes, *Journal*

of Geophysical Research, 116(B5), doi:10.1029/2010JB007788.

Fialko, Y. (2006), Interseismic strain accumulation and the earthquake potential on the southern San Andreas fault system, *Nature*, 441(7096), 968–971, doi:

10.1038/nature04797.

Fossen, H., and A. Rotevatn (2016), Fault linkage and relay structures in extensional settings-A review, *Earth-Science Reviews*, 154, 14–28, doi:

10.1016/j.earscirev.2015.11.014.

Freed, A. M. (2005), Earthquake Triggering By Static, Dynamic, and Postseismic Stress Transfer, *Annual Review of Earth and Planetary Sciences*, 33(1), 335–367, doi:

10.1146/annurev.earth.33.092203.122505.

Galli, P. A., B. Giaccio, P. Messina, E. Peronace, and G. M. Zuppi (2011), Palaeoseismology of the L'Aquila faults (central Italy, 2009, Mw 6.3 earthquake): Implica-

tions for active fault linkage, *Geophysical Journal International*, 187(3), 1119–1134, doi:10.1111/j.1365-246X.2011.05233.x.

Ganas, A., E. Sokos, A. Agalos, G. Leontakianakos, and S. Pavlides (2006), Coulomb stress triggering of earthquakes along the Atalanti Fault, central Greece: Two April 1894 M6+ events and stress change patterns, *Tectonophysics*, *420*(3), 357–369, doi:10.1016/j.tecto.2006.03.028.

Gawthorpe, R. L. (1987), Tectono-sedimentary evolution of the Bowland Basin, N England, during the Dinantian, *Journal of the Geological Society*, *144*, 59–71.

Gawthorpe, R. L., and J. M. Hurst (1993), Transfer zones in extensional basins: their structural style and influence on drainage development and stratigraphy, *Journal of the Geological Society*, *150*, 1137–1152.

Giba, M., J. Walsh, and A. Nicol (2012), Segmentation and growth of an obliquely reactivated normal fault, *Journal of Structural Geology*, *39*, 253–267, doi:10.1016/j.jsg.2012.01.004.

Gomberg, J. (1996), Stress/strain changes and triggered seismicity following the Mw 7.3 Landers, California, earthquake, *Journal of geophysical research*, *101*(B1), 751–764, doi:10.1029/95JB03251.

Gomberg, J. (2001), The failure of earthquake failure models, *Journal of Geophysical Research*, *106*(B8), 16,253, doi:10.1029/2000JB000003.

Gomberg, J., N. M. Beeler, M. L. Blanpied, and P. Bodin (1998), Earthquake triggering by transient and static deformations, *Journal of Geophysical Research*, *103*(B10), 24,411, doi:10.1029/98JB01125.

Gomberg, J., P. a. Reasenber, P. Bodin, and R. a. Harris (2001), Earthquake triggering by seismic waves following the Landers and Hector Mine earthquakes., *Nature*, *411*(6836), 462–466, doi:10.1038/35078053.

Gupta, A., and C. H. Scholz (2000), A model of normal fault interaction based on observations and theory, *Journal of Structural Geology*, *22*(7), 865–879, doi:10.1016/S0191-8141(00)00011-0.

Hamling, I. J., S. Hreinsdóttir, K. Clark, J. Elliott, C. Liang, E. Fielding, N. Litchfield, P. Villamor, L. Wallace, T. J. Wright, E. D’Anastasio, S. Bannister, D. Burbidge, P. Denys, P. Gentle, J. Howarth, C. Mueller, N. Palmer, C. Pearson, W. Power, P. Barnes, D. J. A. Barrell, R. Van Dissen, R. Langridge, T. Little, A. Nicol, J. Pettinga, J. Rowland, and M. Stirling (2017), Complex multifault rupture during the 2016 M w 7.8 Kaikoura earthquake, New Zealand, *Science*, *7194*(April), eaam7194, doi:10.1126/science.aam7194.

Harris, R. a. (1998), Introduction to Special Section: Stress Triggers, Stress Shadows, and Implications for Seismic Hazard, *Journal of Geophysical Research*, *103*(B10), 24,347, doi:10.1029/98JB01576.

Harris, R. A., and S. M. Day (1993), Dynamics of Fault Interaction : Parallel Strike-Slip Faults, *Journal of Geophysical Research*, *98*(B3), 4461–4472.

Harris, R. A., and S. M. Day (1999), Dynamic 3D simulations of earthquakes on en echelon faults, *Journal of Geophysical Research*, *26*(14), 2089–2092.

Harris, R. A., and R. W. Simpson (1992), Changes in static stress on southern California faults after the 1992 Landers earthquake, *Nature*, *360*(6401), 251–254, doi:10.1038/360251a0.

Harris, R. a., and R. W. Simpson (1996), In the shadow of 1857-the effect of the Great Ft. Tejon Earthquake on subsequent earthquakes in southern California, *Geophysical Research Letters*, *23*(3), 229, doi:10.1029/96GL00015.

Hatem, A. E., M. L. Cooke, and E. H. Madden (2015), Evolving efficiency of restraining bends within wet kaolin analog experiments, *Journal of Geophysical Research: Solid Earth*, *120*, 1975–1992, doi:10.1002/2014JB011735.

Hayes, G. P., R. W. Briggs, A. Sladen, E. J. Fielding, C. Prentice, K. Hudnut, P. Mann, F. W. Taylor, a. J. Crone, R. Gold, T. Ito, and M. Simons (2010), Complex rupture during the 12 January 2010 Haiti earthquake, *Nature Geoscience*, *3*(11), 800–805, doi:10.1038/ngeo977.

Herbert, J. W., M. L. Cooke, P. Souloumiac, E. H. Madden, B. C. L. Mary, and B. Mailhot (2015), The work of fault growth in laboratory sandbox experiments, *Earth and Planetary Science Letters*, *432*, 95–102, doi:10.1016/j.epsl.2015.09.046.

Hill, P., M. J. S. Johnston, and J. O. Langbein (1995), Response of Long Valley caldera to the Mw - 7.3 Landers, California, Earthquake, *Journal of Geophysical Research*, *100*, 12,985–13,005.

Hodge, M., J. Biggs, K. Goda, and W. Aspinall (2015), Assessing infrequent large earthquakes using geomorphology and geodesy: the Malawi Rift, *Natural Hazards*, pp. 1–26, doi:10.1007/s11069-014-1572-y.

Ikari, M. J., C. Marone, and D. M. Saffer (2011), On the relation between fault strength and frictional stability, *Geology*, *39*(1), 83–86, doi:10.1130/G31416.1.

Kase, Y. (2010), Slip-length scaling law for strike-slip multiple segment earthquakes based on dynamic rupture simulations, *Bulletin of the Seismological Society of America*, *100*(2), 473–481, doi:10.1785/0120090090.

Kijko, a., and G. Graham (1998), Parametric-historic Procedure for Probabilistic Seismic Hazard Analysis Part I: Estimation of Maximum Regional Magnitude m_{max} , *Pure and*

Applied Geophysics, 152, 413–442, doi:10.1007/s000240050161.

Kilb, D., J. Gomberg, and P. Bodin (2000), Triggering of earthquake aftershocks by dynamic stresses., *Nature*, 408(6812), 570–574, doi:10.1038/35046046.

King, G., and J. Nabelek (1985), Role of fault bends in the initiation and termination of earthquake rupture., *Science*, 228(4702), 984–987, doi:10.1126/science.228.4702.984.

King, G., S. Stein, and J. Lin (1994), Static stress changes and the triggering of earthquakes, *Bulletin of the Seismological Society of America*, 84(3), 935–953, doi:10.1016/0148-9062(95)94484-2.

King, G. C. P., and M. Cocco (2001), Fault interaction by elastic stress changes: New clues from earthquake sequences, doi:10.1016/S0065-2687(00)80006-0.

Kristensen, M. B., C. J. Childs, and J. A. Korstgard (2008), The 3D geometry of small-scale relay zones between normal faults in soft sediments, *Journal of Structural Geology*, 30(2), 257–272, doi:10.1016/j.jsg.2007.11.003.

Laó-Dávila, D. A., H. S. Al-Salmi, M. G. Abdelsalam, and E. A. Atekwana (2015), Hierarchical segmentation of the Malawi Rift: The influence of inherited lithospheric heterogeneity and kinematics in the evolution of continental rifts, *Tectonics*, 34, 2399–2417, doi:10.1002/2015TC003953.

Larsen, P. H. (1988), Relay structures in a Lower Permian basement- involved extension system, East Greenland, *Journal of Structural Geology*, 10(1), 3–8, doi:10.1016/0191-8141(88)90122-8.

Lezzar, K. E., J.-J. Tiercelin, C. Le Turdu, A. S. Cohen, D. J. Reynolds, B. Le Gall, and C. A. Scholz (2002), Control of normal fault interaction on the distribution of major Neogene sedimentary depocenters, Lake Tanganyika, East African rift, *AAPG bulletin*,

86(6), 1027–1060.

Lin, J., and R. S. Stein (2004), Stress triggering in thrust and subduction earthquakes and stress interaction between the southern San Andreas and nearby thrust and strike-slip faults, *Journal of Geophysical Research*, *109*(B2), 1–19, doi:10.1029/2003JB002607.

Long, J. J., and J. Imber (2012), Strain compatibility and fault linkage in relay zones on normal faults, *Journal of Structural Geology*, *36*, 16–26, doi:10.1016/j.jsg.2011.12.013.

Lozos, J. C., D. D. Oglesby, J. N. Brune, and K. B. Olsen (2012), Small intermediate fault segments can either aid or hinder rupture propagation at stepovers, *Geophysical Research Letters*, *39*(17), 5–8, doi:10.1029/2012GL053005.

Lozos, J. C., D. D. Oglesby, J. N. Brune, and K. B. Olsen (2015), Rupture propagation and ground motion of strike-slip stepovers with intermediate fault segments, *Bulletin of the Seismological Society of America*, *105*(1), 387–399, doi:10.1785/0120140114.

Luccio, F. D., G. Ventura, R. D. Giovambattista, A. Piscini, and F. R. Cinti (2010), Normal faults and thrusts reactivated by deep fluids : The 6 April 2009 Mw 6.3 L'Aquila earthquake , central Italy, *Journal of Geophysical Research*, *115*(3), doi:10.1029/2009JB007190.

Manighetti, I., M. Campillo, S. Bouley, and F. Cotton (2007), Earthquake scaling, fault segmentation, and structural maturity, *Earth and Planetary Science Letters*, *253*, 429–438, doi:10.1016/j.epsl.2006.11.004.

Manighetti, I., D. Zigone, M. Campillo, and F. Cotton (2009), Self-similarity of the largest-scale segmentation of the faults: Implications for earthquake behavior, *Earth and Planetary Science Letters*, *288*(3-4), 370–381, doi:10.1016/j.epsl.2009.09.040.

Manighetti, I., C. Caulet, D. De Barros, C. Perrin, F. Cappa, and Y. Gaudemer (2015), Generic along-strike segmentation of Afar normal faults, East Africa: Implications on fault growth and stress heterogeneity on seismogenic fault planes, *Geochem. Geophys. Geosyst.*, *16*, 443–467, doi:10.1002/2014GC005691. Received.

Martinez-Martinez, J. M., G. Booth-Rea, J. M. Azanon, and F. Torcal (2006), Active transfer fault zone linking a segmented extensional system (Betics, southern Spain): Insight into heterogeneous extension driven by edge delamination, *Tectonophysics*, *422*(1–4), 159–173, doi:10.1016/j.tecto.2006.06.001.

McBeck, J. A., E. H. Madden, and M. L. Cooke (2016), Growth by Optimization of Work (GROW): A new modeling tool that predicts fault growth through work minimization, *Computers & Geosciences*, *88*, 142–151.

McClay, K., and S. Khalil (1998), Extensional hard linkages, eastern Gulf of Suez, Egypt, *Geology*, *26*(6), 563–566, doi:10.1130/0091-7613(1998)026<0563:EHLEGO>2.3.CO;2.

Morewood, N. C., and G. P. Roberts (1999), Lateral propagation of the surface trace of the South Alkyonides normal fault segment, central Greece: Its impact on models of fault growth and displacement-length relationships, *Journal of Structural Geology*, *21*(6), 635–652, doi:10.1016/S0191-8141(99)00049-8.

Morley, C. (1999a), How successful are analogue models in addressing the influence of pre-existing fabrics on rift structure?, *Journal of Structural Geology*, *21*, 1267–1274.

Morley, C. K. (1999b), Marked along-strike variations in dip of normal faults—the Lokichar fault, N. Kenya rift: A possible cause for metamorphic core complexes, *Journal of Structural Geology*, *21*, 479–492, doi:10.1016/S0191-8141(99)00043-7.

Morley, C. K. (2010), Stress re-orientation along zones of weak fabrics in rifts: An explanation for pure extension in 'oblique' rift segments?, *Earth and Planetary Science Letters*, 297(3-4), 667–673, doi:10.1016/j.epsl.2010.07.022.

Morley, C. K., R. A. Nelson, T. L. Patton, and S. G. Munn (1990), Transfer zones in the East African Rift system and their relevance to hydrocarbon exploration in rifts, *AAPG Bulletin*, 74(8), 1234–1253.

Morley, C. K., C. Haranya, W. Phoosongsee, S. Pongwapee, A. Kornawan, and N. Wonganan (2004), Activation of rift oblique and rift parallel pre-existing fabrics during extension and their effect on deformation style: Examples from the rifts of Thailand, *Journal of Structural Geology*, 26, 1803–1829, doi:10.1016/j.jsg.2004.02.014.

Murray, J., and P. Segall (2002), Testing time-predictable earthquake recurrence by direct measurement of strain accumulation and release, *Nature*, 414, 287–291, doi:10.1038/nature01021.1.

Nicol, A., J. Walsh, K. Berryman, and S. Nodder (2005), Growth of a normal fault by the accumulation of slip over millions of years, *Journal of Structural Geology*, 27, 327–342, doi:10.1016/j.jsg.2004.09.002.

Nicol, a., J. Walsh, P. Villamor, H. Seebeck, and K. Berryman (2010), Normal fault interactions, paleoearthquakes and growth in an active rift, *Journal of Structural Geology*, 32(8), 1101–1113, doi:10.1016/j.jsg.2010.06.018.

Noda, H., N. Lapusta, and H. Kanamori (2013), Comparison of average stress drop measures for ruptures with heterogeneous stress change and implications for earthquake physics, *Geophysical Journal International*, 193(3), 1691–1712, doi:10.1093/gji/ggt074.

Okada, Y. (1992), Internal deformation due to shear and tensile faults in half-space, *Bulletin of the Seismological Society of America*, *82*(2), 1018–1040.

Otsuki, K., and T. Dilov (2005), Evolution of hierarchical self-similar geometry of experimental fault zones : Implications for seismic nucleation and earthquake size, *Journal of Geophysical Research*, *110*, 1–9, doi:10.1029/2004JB003359.

Peacock, D. (2002), Propagation, interaction and linkage in normal fault systems, *Earth-Science Reviews*, *58*(1-2), 121–142, doi:10.1016/S0012-8252(01)00085-X.

Peacock, D., and D. Sanderson (1991), Displacements, segment linkage and relay ramps in normal fault zones, *Journal of Structural Geology*, *13*(6), 721–733, doi:10.1016/0191-8141(91)90033-F.

Peacock, D. C. P., and E. A. Parfitt (2002), Active relay ramps and normal fault propagation on Kilauea Volcano, Hawaii, *Journal of Structural Geology*, *24*(4), 729–742, doi:10.1016/S0191-8141(01)00109-2.

Peacock, D. C. P., and D. J. Sanderson (1994), Geometry and development of relay ramps in normal fault systems, *AAPG bulletin*, *78*(2), 147–165.

Peltzer, G., F. Crampé, S. Hensley, and P. Rosen (2001), Transient strain accumulation and fault interaction in the Eastern California shear zone, *Geology*, *29*(11), 975–978.

Perrin, C., I. Manighetti, and Y. Gaudemer (2016), Off-fault tip splay networks : A genetic and generic property of faults indicative of their long-term propagation, *Comptes Rendus Geoscience*, *348*, 52–60.

Pollard, D. D., and P. Segall (1987), Theoretical displacements and stresses near fractures in rock: with applications to faults, joints, veins, dikes, and solution surfaces, *Fracture mechanics of rock*, *277*(349), 277–349.

Reeve, M. T., R. E. Bell, O. B. Duffy, C. A. Jackson, and E. Sansom (2015), The growth of non-colinear normal fault systems; What can we learn from 3D seismic reflection data?, *Journal of Structural Geology*, *70*, 141–155, doi:10.1016/j.jsg.2014.11.007.

Ring, U. (1994), The influence of preexisting structure on the evolution of the Cenozoic Malawi rift (East African rift system), *Tectonics*, *13*(2), 313–326.

Rosendahl, B. (1987), Architecture of Continental Rifts with special reference to East Africa, *Annual Review of Earth and Planetary Sciences*, *15*, 445–503.

Rotevatn, A., and E. Bastesen (2014), Fault linkage and damage zone architecture in tight carbonate rocks in the Suez Rift (Egypt): implications for permeability structure along segmented normal faults, *Geological Society, London, Special Publications*, *374*(1), 79–95, doi:10.1144/SP374.12.

Rudnicki, J. W. (1980), Fracture Mechanics Applied to the Earth's Crust, *Annual Review of Earth and Planetary Sciences*, *8*, 489–525, doi:10.1146/annurev.ea.08.050180.002421.

Sagy, A., E. E. Brodsky, and G. J. Axen (2007), Evolution of fault-surface roughness with slip, *Geology*, *35*(3), 283–286, doi:10.1130/G23235A.1.

Savage, H. M., and E. E. Brodsky (2011), Collateral damage: Evolution with displacement of fracture distribution and secondary fault strands in fault damage zones, *Journal of Geophysical Research*, *116*(B3), B03,405, doi:10.1029/2010JB007665.

Scholz, C. (2002), *The mechanics of earthquakes and faulting*, Cambridge university press.

Scholz, C. H., R. Ando, and B. E. Shaw (2010), The mechanics of first order splay faulting: The strike-slip case, *Journal of Structural Geology*, *32*(1), 118–126, doi:10.1016/j.jsg.2009.10.007.

Schultz, R. a., R. Soliva, H. Fossen, C. H. Okubo, and D. M. Reeves (2008), Dependence of displacement-length scaling relations for fractures and deformation bands on the volumetric changes across them, *Journal of Structural Geology*, *30*(11), 1405–1411, doi:10.1016/j.jsg.2008.08.001.

Schwartz, D. P., and K. J. Coppersmith (1984), Fault behavior and characteristic earthquakes: Examples from the Wasatch and San Andreas Fault Zones, *Journal of Geophysical Research*, *89*(B7), 5681, doi:10.1029/JB089iB07p05681.

Segall, P., and D. D. Pollard (1980), Mechanics of discontinuous faults, *Journal of Geophysical Research: Solid Earth (1978–2012)*, *85*(B8), 4337–4350.

Shaw, B. E., and C. H. Scholz (2001), Slip-length scaling in large earthquakes: Observations and theory and implications for earthquake physics, *Geophysical Research Letters*, *28*(15), 2995–2998, doi:10.1029/2000GL012762.

Shen, Z.-K., J. Sun, P. Zhang, Y. Wan, M. Wang, R. Bürgmann, Y. Zeng, W. Gan, H. Liao, and Q. Wang (2009), Slip maxima at fault junctions and rupturing of barriers during the 2008 Wenchuan earthquake, *Nature Geoscience*, *2*(10), 718–724, doi:10.1038/ngeo636.

Sieh, K., L. Jones, E. Hauksson, K. Hudnut, D. Eberhart-Phillips, T. Heaton, S. Hough, K. Hutton, H. Kanamori, A. Lilje, S. Lindvall, S. F. McGill, J. Mori, C. Rubin, J. a. Spotila, J. Stock, H. K. Thio, J. Treiman, B. Wernicke, and J. Zachariassen (1993), Near-field investigations of the landers earthquake sequence, april to july 1992., *Science (New York, N.Y.)*, *260*(5105), 171–176, doi:10.1126/science.260.5105.171.

Soliva, R., and A. Benedicto (2004), A linkage criterion for segmented normal faults, *Journal of Structural Geology*, *26*(12), 2251–2267, doi:10.1016/j.jsg.2004.06.008.

Stein, R. S. (1999), The role of stress transfer in earthquake occurrence, *Nature*, 402(6762), 605–609, doi:10.1038/45144.

Stein, R. S., A. A. Barka, and J. H. Dieterich (1997), Earthquake Stress Triggering, *Geophysical Journal International*, pp. 594–604.

Taylor, S. K., J. M. Bull, G. Lamarche, and P. M. Barnes (2004), Normal fault growth and linkage in the Whakatane Graben, New Zealand, during the last 1.3 Myr, *Journal of Geophysical Research: Solid Earth*, 109(B2), 1–22, doi:10.1029/2003JB002412.

Toda, S., J. Lin, and R. S. Stein (2011), Using the 2011 Mw 9.0 off the Pacific coast of Tohoku Earthquake to test the Coulomb stress triggering hypothesis and to calculate faults brought closer to failure, *Earth, Planets and Space*, 63(7), 725–730, doi:10.5047/eps.2011.05.010.

Trudgill, B., and J. Cartwright (1994), Relay-ramp forms and normal-fault linkages, Canyonlands National Park, Utah, *Geological Society of America Bulletin*, 106(9), 1143–1157.

Walsh, J. J., and J. Watterson (1991), Geometric and kinematic coherence and scale effects in normal fault systems, *Geological Society, London, Special Publications*, 56(1), 193–203, doi:10.1144/GSL.SP.1991.056.01.13.

Walsh, J. J., A. Nicol, and C. Childs (2002), An alternative model for the growth of faults, *Journal of Structural Geology*, 24(11), 1669–1675, doi:10.1016/S0191-8141(01)00165-1.

Walsh, J. J., W. R. Bailey, C. Childs, A. Nicol, and C. G. Bonson (2003), Formation of segmented normal faults: A 3-D perspective, *Journal of Structural Geology*, 25(8), 1251–1262, doi:10.1016/S0191-8141(02)00161-X.

Wedmore, L. N. J., J. P. Faure Walker, G. P. Roberts, P. R. Sammonds, K. J. W. McCaffrey, and P. A. Cowie (2017), A 667-year record of co-seismic and interseismic Coulomb stress changes in central Italy reveals the role of fault interaction in controlling irregular earthquake recurrence intervals, *Journal of Geophysical Research Solid Earth*, *122*, 1–21, doi:10.1002/2017JB014054.

Wells, D., and K. Coppersmith (1994), New empirical relationships among magnitude, rupture length, rupture width, rupture area, and surface displacement, *Bulletin of the Seismological Society of America*, *84*(4), 974–1002.

Wesnousky, S. G. (1986), Earthquakes, Quaternary faults, and seismic hazard in California, *Journal of Geophysical Research*, *91*(B12), 12,587–12,631.

Wesnousky, S. G. (1988), Seismological and structural evolution of strike-slip faults, doi:10.1038/335340a0.

Wesnousky, S. G. (2008), Displacement and geometrical characteristics of earthquake surface ruptures: Issues and implications for seismic-hazard analysis and the process of earthquake rupture, *Bulletin of the Seismological Society of America*, *98*(4), 1609–1632, doi:10.1785/0120070111.

Whipp, P. S., C. a. L. Jackson, R. L. Gawthorpe, T. Dreyer, and D. Quinn (2014), Normal fault array evolution above a reactivated rift fabric; a subsurface example from the northern Horda Platform, Norwegian North Sea, *Basin Research*, *26*(4), 523–549, doi:10.1111/bre.12050.

Wilcox, R. E., T. P. t. Harding, and D. R. Seely (1973), Basic wrench tectonics, *Aapg Bulletin*, *57*(1), 74–96.

Willemse, E. J. M. (1997), Segmented normal faults: Correspondence between three-dimensional mechanical models and field data, *Journal of Geophysical Research*, *102*(B1), 675, doi:10.1029/96JB01651.

Willemse, E. J. M., D. D. Pollard, and A. Aydin (1996), Three-dimensional analyses of slip distributions on normal fault arrays with consequences for fault scaling, *Journal of Structural Geology*, *18*(2/3), 295–309.

Withjack, M. O., and W. R. Jamison (1986), Deformation produced by oblique rifting, *Tectonophysics*, *126*(2-4), 99–124, doi:10.1016/0040-1951(86)90222-2.

Young, M. J., R. L. Gawthorpe, and S. Hardy (2001), Growth and linkage of a segmented normal fault zone; the Late Jurassic Murchison-Statfjord North Fault, Northern North Sea, *Journal of Structural Geology*, *23*(12), 1933–1952.

Youngs, R. R., and K. J. Coppersmith (1985), Implications of fault slip rates and earthquake recurrence models to probabilistic seismic hazard estimates, *Bulletin of the Seismological society of America*, *75*(4), 939–964.

Zhang, P., D. B. Slemmons, and F. Mao (1991), Geometric pattern, rupture termination and fault segmentation of the Dixie Valley-Pleasant Valley active normal fault system, Nevada, U.S.A., *Journal of Structural Geology*, *13*(2), 165–176.

Zhao, S., R. D. Müller, Y. Takahashi, and Y. Kaneda (2004), 3-D finite-element modelling of deformation and stress associated with faulting: Effect of inhomogeneous crustal structures, *Geophysical Journal International*, *157*(2004), 629–644, doi:10.1111/j.1365-246X.2004.02200.x.

Ziv, A., and A. M. Rubin (2000), Static stress transfer and earthquake triggering: No lower threshold in sight?, *Journal of Geophysical Research*, *105*(B6), 13,631–13,642,

doi:10.1029/2000JB900081.

Accepted Article

©2017 American Geophysical Union. All Rights Reserved.

Table 1. Examples of geometrical linkage configurations between fault segments for continental normal faults

No.	Fault Name/ Fault Zone	Location	Segment 1 (km)	Segment 2 (km)	Overlap (km)	Separation (km)	α ($^{\circ}$)	θ ($^{\circ}$)	Ref
1) Fault Bends									
(1)	Abadare Fault	Gregory Rift, East Africa	65.0	20.0	-20.0	10.0	27	27	1
(2)	Gulf of Evvia Fault Zone	The Gulf of Evvia, Atalanti	7.7	5.5	-0.7	0.7	45	45	1
(3)	Fayette Fault	Wasatch Fault Zone, Salt Lake City	12.7	8.8	-3.1	2.5	39	39	1
(4)	Nguruman Fault	Gregory Rift, East Africa	20.0	15.5	-8.5	4.0	25	25	1
(5)	Atalanti Fault	Atalanti Fault Zone, Central Greece	11.2	6.2	-3.7	1.6	24	24	2
(6)	Skinos Fault	Gulf of Corinth, Central Greece	6.3	5.3	-1.8	0.8	24	24	3
2) Breached Ramps									
(7)	Parihaka Fault	Taranaki Basin, New Zealand	10.2	8.4	2.1	1.4	34	146	4
(8)	Marcusdal Relay Ramp	East Greenland	18.5	15.8	3.0	4.1	54	126	5
(9)	Holger Danske Relay Ramp	East Greenland	18.5	9.5	1.7	3.0	61	120	5
(10)	Deer Fault	Utah	0.6	0.4	0.1	0.1	34	135	6
(11)	Summer Lake Basin	Oregon	5.0	2.2	1.1	0.5	24	156	7
(12)	Murchison-Statfjord North Fault	Northern North Sea	25.0	10.0	1.4	1.9	55	126	8
(13)	Hilina Fault System	Big Island, Hawaii	16.9	16.8	7.4	4.8	33	147	9
(14)	Pearce and Tobin Faults	Pleasant Valley, Nevada	28.0	9.2	1.4	5.0	74	112	1
3) Transform Faults									
(15)	Gulf of Evvia Fault Zone	The Gulf of Evvia, Atalanti	18.2	11.3	-1.8	3.6	63	63	1
(16)	Bare Mountain Fault Zone	Crater flat area, Southwestern Nevada	6.9	3.8	-0.9	1.6	61	61	10
(17)	Rusizi Rift System	East Africa	10.4	7.3	0.5	2.7	87	100	11
(18)	Rio Grande Rift System	Colorado, New Mexico	44.8	30.2	-11.6	39.0	73	73	12
(19)	North Craven and Middle Craven Faults	Bowland Basin, Northern England	19.8	10.0	1.3	25.0	87	93	13
(20)	Central Betics Fault Zone	Betics, Southern Spain	4.0	2.6	-0.2	1.2	79	81	14

1: Gawthorpe and Hurst [1993], 2: Ganas et al. [2006], 3: Duffy et al. [2014], 4: Giba et al. [2012], 5: Larsen [1988],
6: Commins et al. [2005], 7: Crider [2001], 8: Young et al. [2001], 9: Peacock and Parfitt [2002], 10: Faulds and Varga [1998],
11: Acocella et al. [1999], 12: Aldrich et al. [1986], 13: Gawthorpe [1987], 14: Martinez-Martinez et al. [2006]

Table 2. End-member receiver fault geometries where the source fault strikes 0° and dips 60°W

	Geometry	Slip	Strike	Dip	Slip Vector Rake
i)	Fault Bend	Normal	θ	60°W	-90°
ii)	Breached Ramp	Normal	45°	60°NW	-90°
iii)	Transform	Strike-Slip	90°	90°	0°
iv)	Along-strike	Normal	0°	60°W	-90°

$\theta = \tan^{-1}(S/U)$ for underlapping faults,
or $\theta = \tan^{-1}(S/O)$ for overlapping faults.

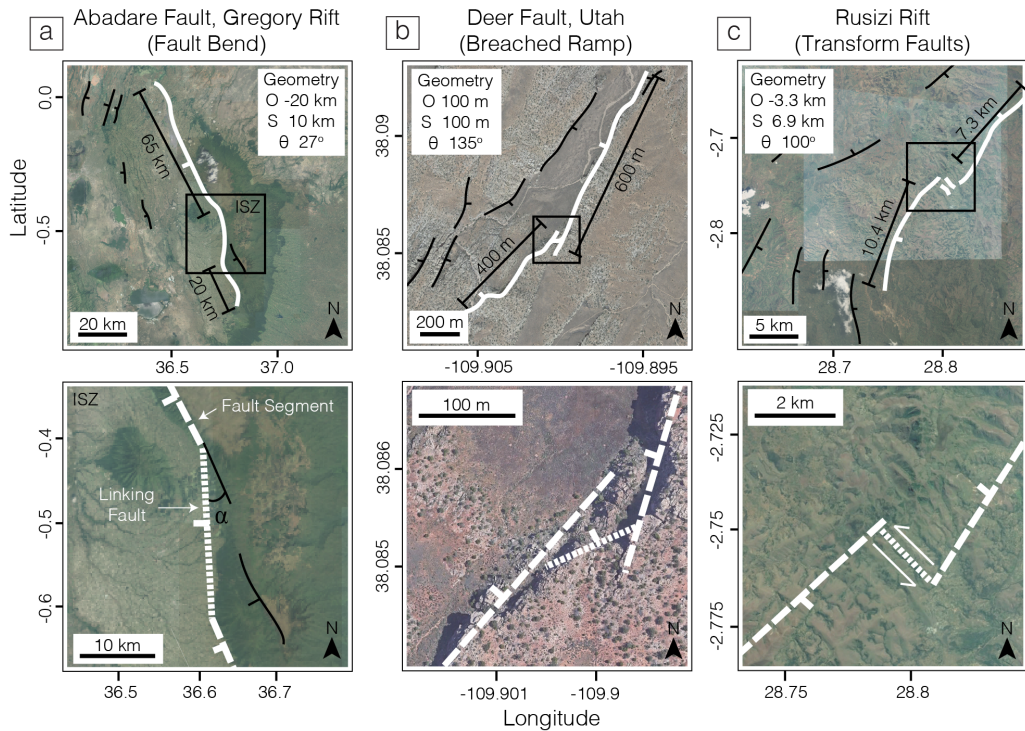


Figure 1. Examples of hard-links between normal fault segments: a) A fault bend ($\alpha \sim 27^\circ$) on the Abadare Fault, Gregory Rift, East Africa [Gawthorpe and Hurst, 1993]; b) A breached relay ramp ($\alpha \sim 34^\circ$) on Deer Fault, Utah, USA [Commins et al., 2005]; c) A transform zone ($\alpha \sim 87^\circ$) across faults in the Rusizi Rift, East Africa [Acocella et al., 1999]. Zoomed in map-view images of the inter-segment zone (ISZ) and end-member linking fault geometries are shown on the bottom panel. Images taken from Google Earth.

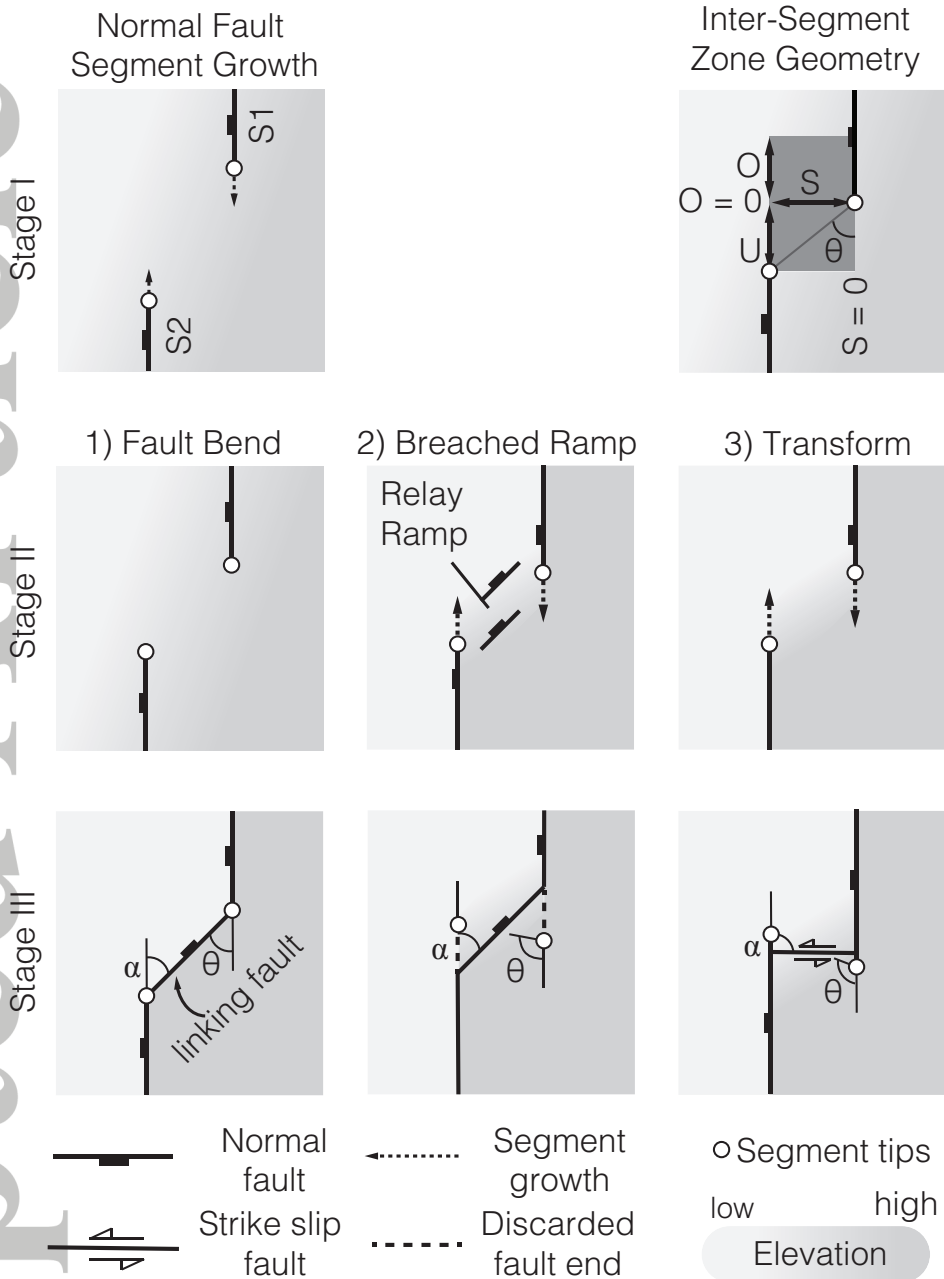


Figure 2. Development of end-member linking fault configurations between parallel normal fault segments: 1) fault bend; 2) breached ramp; and 3) transform fault. Stage I shows incremental growth of one, or both, fault segments. 1) For fault bends, segment geometry begins to be influenced by the adjacent fault segment (Stage II); the linking fault then develops with strike at angle α (equal to θ) to the strike of the segments (Stage III). 2) For breached ramps, displacement becomes localised in the relay ramp, then secondary faults nucleate striking at angle α to the strike of the segments (Stage II); one of the secondary faults breach across the ramp, generating the hard-linked connection (Stage III). 3) For transforms, segment growth continues without a change in strike (Stage II), geometry becomes favourable for linkage with a strike-slip transform fault striking at angle α to the strike of the segments (Stage III).

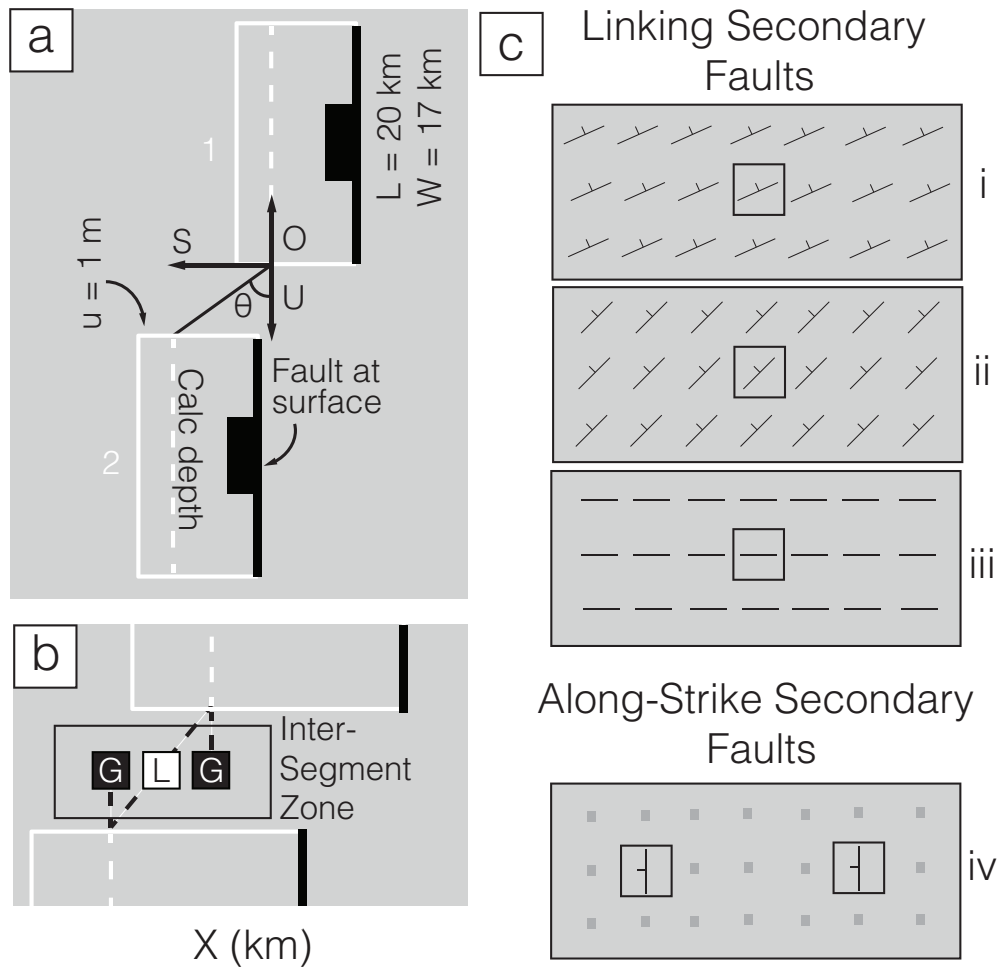


Figure 3. a) Model setup showing the fault segments at the surface (black line), fault plane surface projection (white box), and calculation depth (dotted white line). Distance between fault segments comprises separation (S), the strike-perpendicular distance between the tips of segments, and overlap (O), the along-strike distance (where underlap, U , is negative overlap). The angle between a line joining the segment tips and the strike of the segments, θ , is used in calculating strike for the fault bend configuration. b) The receiver fault location where $\Delta\sigma_c$ is recorded. Linking fault $\Delta\sigma_c$ is taken from 'L', along-strike secondary fault $\Delta\sigma_c$ is taken from point 'G'. c) Map-view of linking fault configurations for: i) fault bends; ii) breached ramps; iii) transform faults; and iv) along-strike secondary faults. The boxes mark where $\Delta\sigma_c$ is taken from.

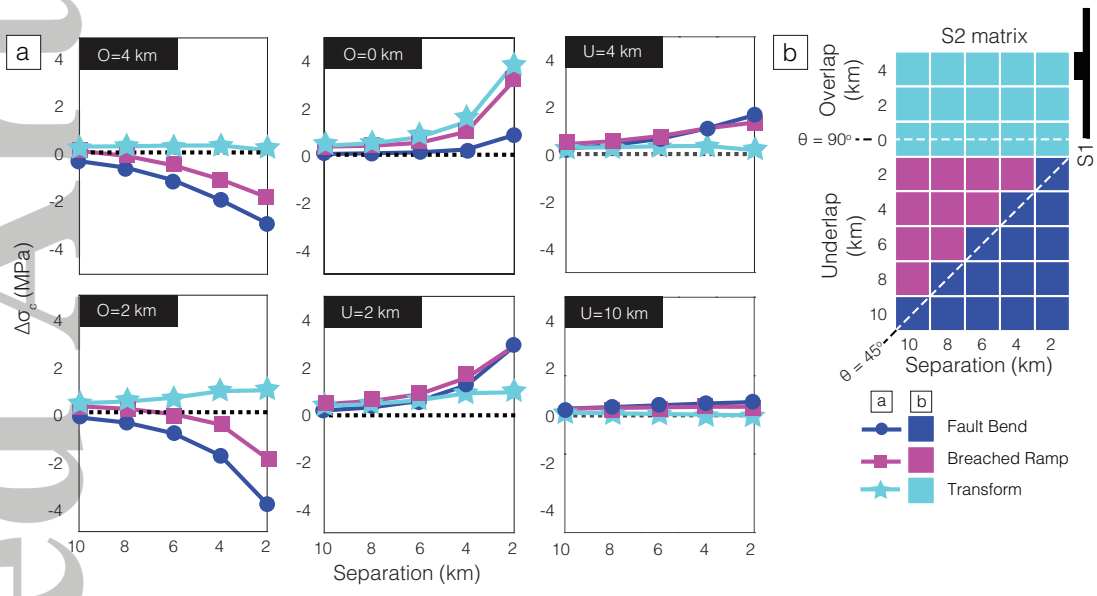


Figure 4. a) Results for linking fault $\Delta\sigma_c$ for the single segment rupture scenario for selected inter-segment zone geometries (see supplementary figure S1 for all geometries). b) Preferred link geometry, that with the largest $\Delta\sigma_c$ magnitude, for the single segment rupture scenario.

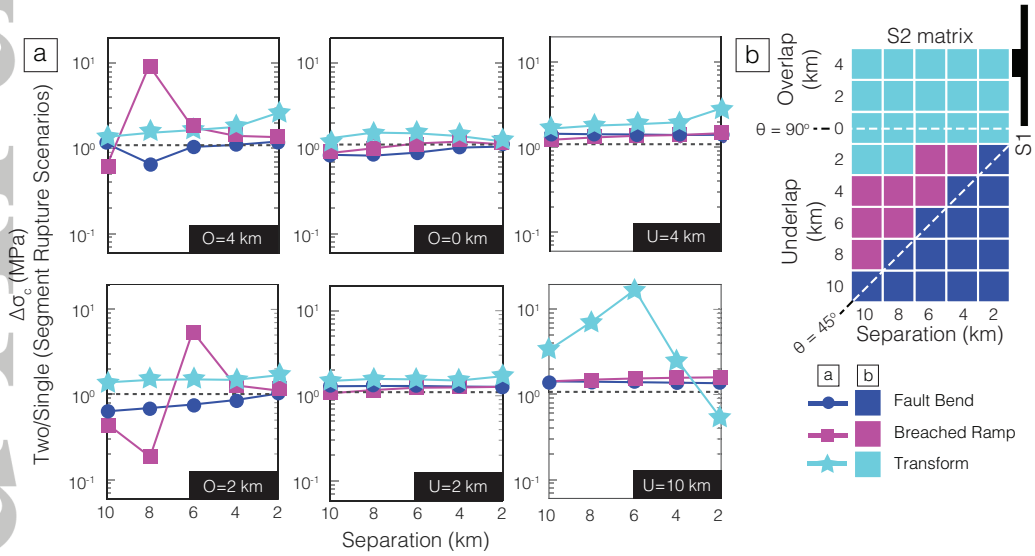


Figure 5. a) The $\Delta\sigma_c$ difference between single and two segment rupture scenarios. A positive difference denotes that the two segment rupture $\Delta\sigma_c$ magnitude was larger. b) Preferred link geometry for two segment rupture scenario. For $\Delta\sigma_c$ results from the two segment rupture scenario, see supplementary figure S2.

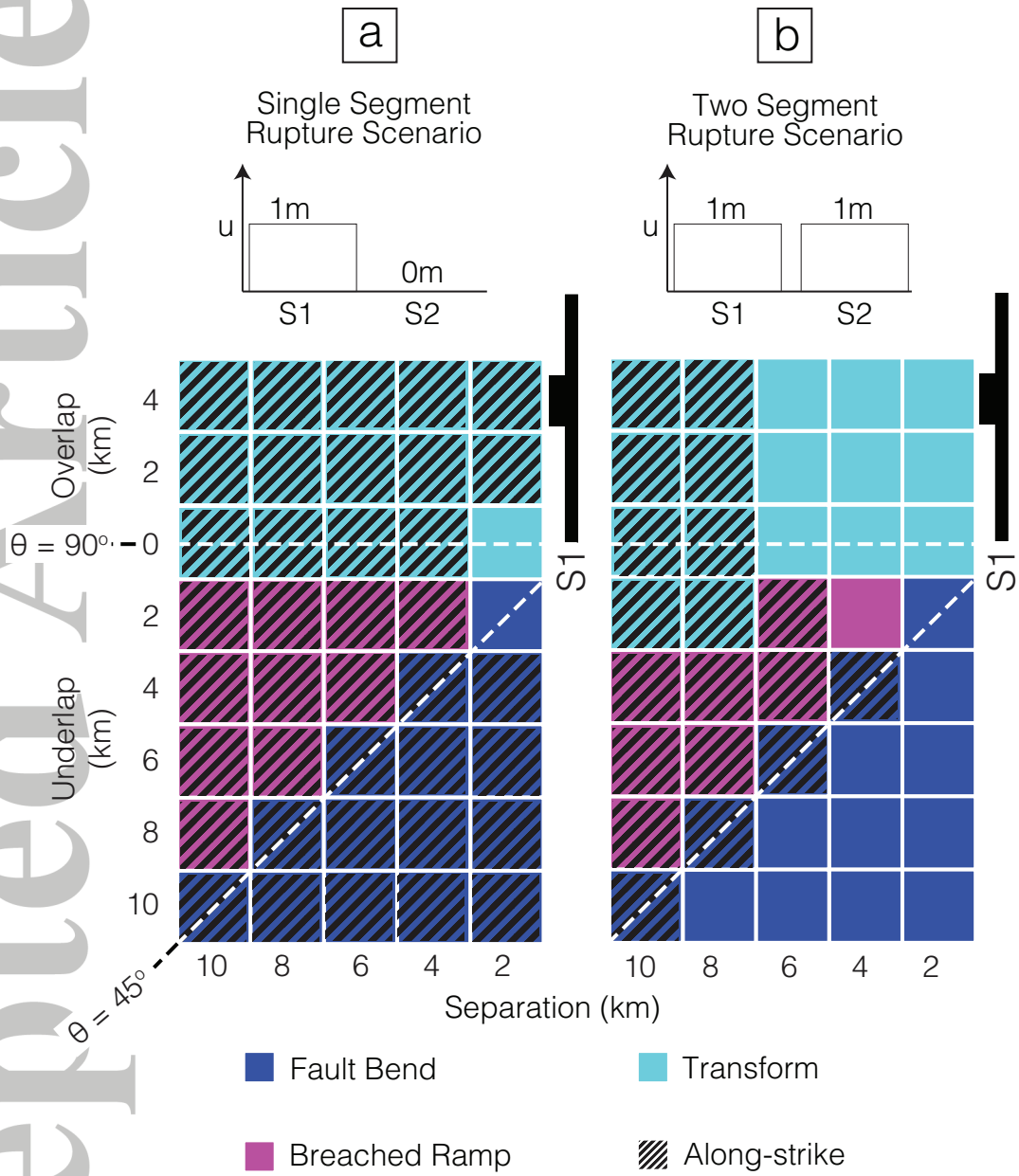


Figure 6. Along-strike secondary fault $\Delta\sigma_c$ compared to linking fault $\Delta\sigma_c$ for a) single and b) two segment rupture scenarios. Diagonal black lines denote the magnitude of the along-strike secondary fault $\Delta\sigma_c$ magnitude was greatest.

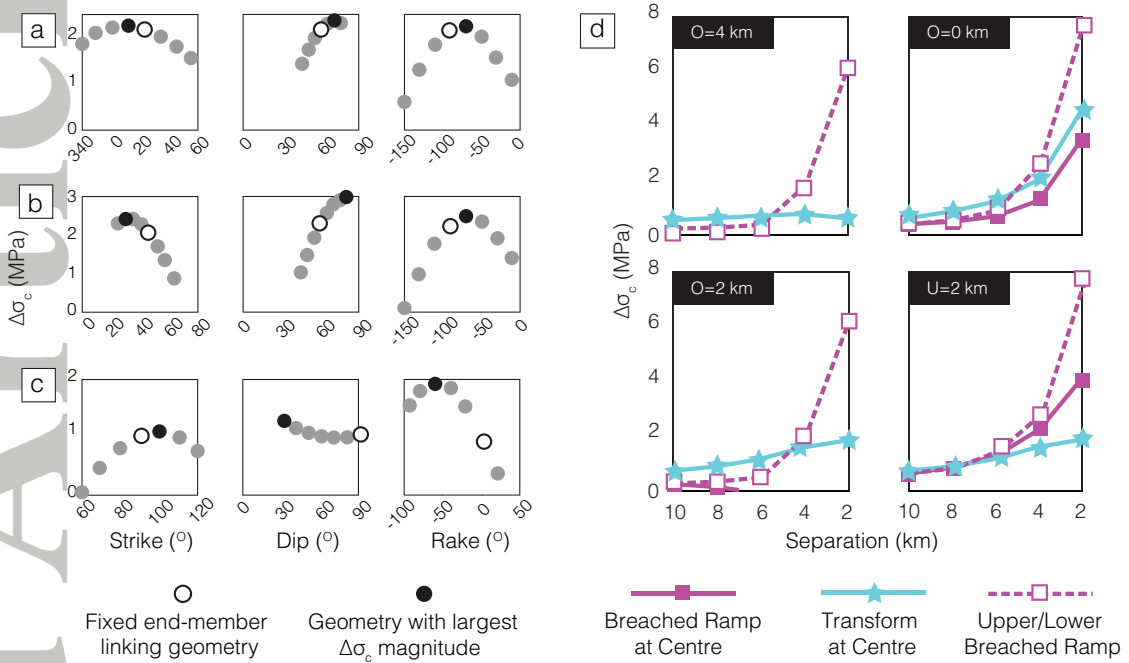


Figure 7. a to c) $\Delta\sigma_c$ based on varying receiver fault strike, dip and slip vector rake. Three geometries were considered, each with a different preferred end-member link geometry: a) fault bend: 4 km underlap and 2 km separation; b) breached ramp: 2 km underlap and 4 km separation; c) transform fault: 2 km overlap and 6 km separation. White circles indicate the $\Delta\sigma_c$ of the preferred fixed end-member linking fault at that inter-segment zone geometry, whereas black circles indicate the linking fault geometry with the largest $\Delta\sigma_c$ magnitude. d) $\Delta\sigma_c$ calculated for relay ramps breached at an optimal location, compared to the $\Delta\sigma_c$ on transform faults and for ramps breached at their centre.

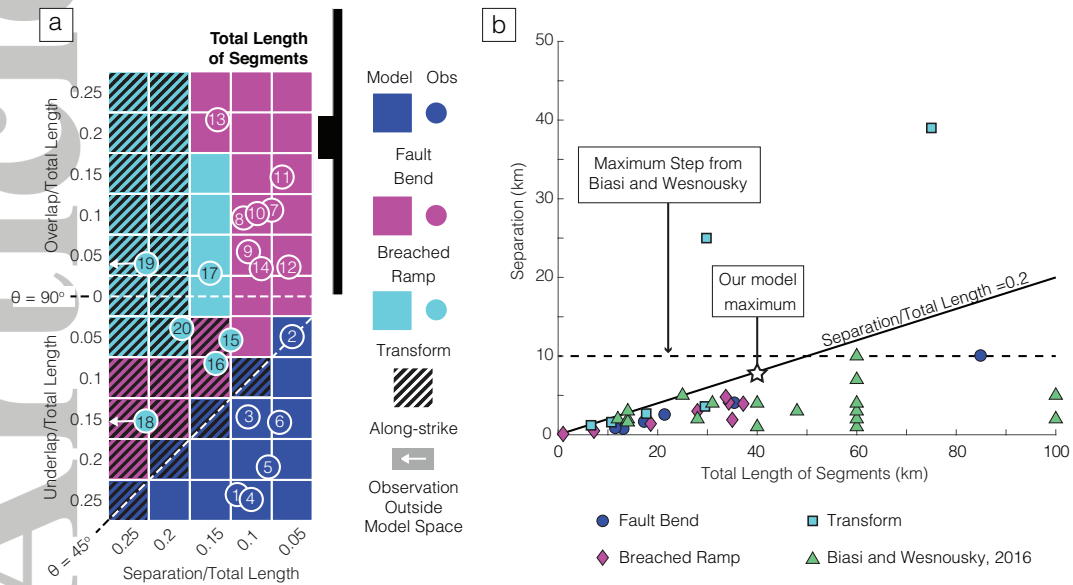


Figure 8. a) Natural observations of hard-links between normal fault segments from Table 1 (numbered) plotted against model predictions of preferred end-member link geometry. Model results are normalised to the length of both segments (40 km), for the two segment rupture scenario, uniform slip distribution run (for tapered slip see Figure S10). Natural observation examples have been normalised to the total length of both segments (for maximum segment and minimum segment length, see Figure S9). Black diagonal lines indicate that along-strike secondary faults are preferred to linking faults between parallel fault segments. Observations that fall outside the model area are shown with an arrow. b) Separation against the length of both segments for natural observations used in this study, and surface rupture examples from *Biasi and Wesnousky, 2016*. Maximum separation is $\sim 20\%$ of the total length of the segments.

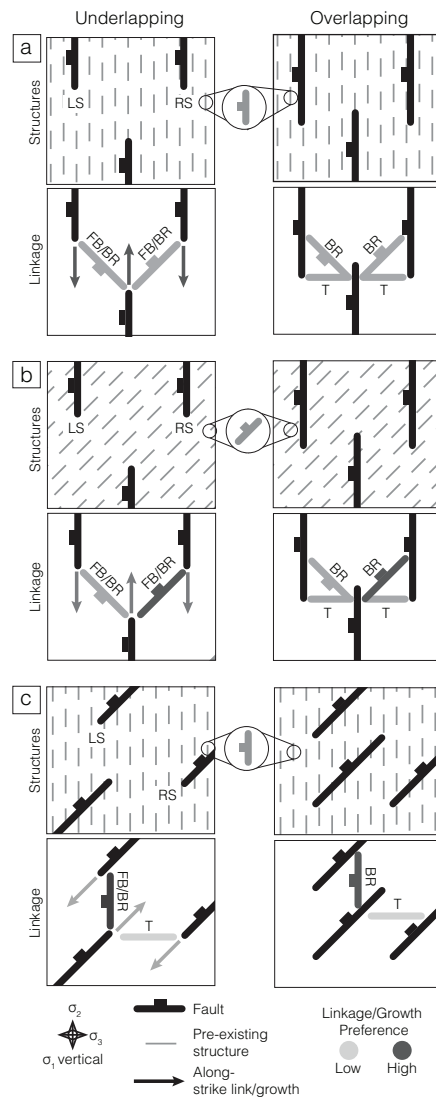


Figure 9. A diagram showing the influence of pre-existing structures on hard-links between normal fault segments. Fault segments (LS, left-stepping, RS, right-stepping) are indicated by thick black lines and pre-existing structures by smaller, grey lines. Both fault segments and pre-existing structures dip at 60° , and the extension direction is E-W. a) Segment and pre-existing structures striking perpendicular to σ_3 . b) Segment strike perpendicular and pre-existing structures strike oblique to σ_3 . c) Both segments and pre-existing structures strike oblique to σ_3 . Geometry of the linking fault between en echelon faults, or along-strike secondary faults, is shown for underlapping and overlapping geometries.